UNIVERSITI PUTRA MALAYSIA

ASSESSING THE PHOTOCATALYTIC PERFORMANCE OF ZIF-8/GRAPHENE TOWARDS LEVOFLOXACIN

CALVIN MANASSEH MANIVEL

ASSESSING THE PHOTOCATALYTIC PERFORMANCE OF ZIF-8/GRAPHENE TOWARDS LEVOFLOXACIN

By

CALVIN MANASSEH A/L MANIVEL

S32695

DEPARTMENT OF SCIENCE AND TECHNOLOGY

FACULTY OF HUMANITIES, MANAGEMENT, AND SCIENCE

UNIVERSITY PUTRA MALAYSIA

2024/2025

ASSESSING THE PHOTOCATALYTIC PERFORMANCE OF ZIF-8/GRAPHENE TOWARDS LEVOFLOXACIN

BY

CALVIN MANASSEH A/L MANIVEL

S32695

PROJECT REPORT SUBMITTED IN PARTIAL FULFILMRNT OF THE REQUIREMENT FOR THE DEGREE OF BACHELOR OD SCIENCE IN INDUSTRIAL CHEMISTRY WITH HONOURS ON THE DEPARTMENT OF SCIENCE AND TECHNOLOGY, FACULTY OF HUMANITIES, MANAGEMENTS AND SCIENCE,

UNIVERSITI PUTRA MALAYSIA

2024/2025

Abstract of thesis presented to the senate of Universiti Putra Malaysia in fulfilment of the requirement for the degree of Bachelor of Science in Industrial Chemistry with Honours.

ASSESSING THE PHOTOCATALYTIC PERFORMANCE OF ZIF-8/GRAPHENE TOWARDS LEVOFLOXACIN

By

CALVIN MANASSEH A/L MANIVEL

January 2025

Chairman : **Alvin Lim Teik Zheng, PhD**

Faculty : **Humanities, Management and Science.**

This study successfully demonstrates the photocatalytic degradation of levofloxacin (LVX) using a ZIF-8/graphene (Gr) composite under simulated low-power UV light irradiation. The ZIF-8/Gr composite outperformed its individual components, achieving superior degradation efficiency by enhancing charge separation, increasing surface area, and improving the production of reactive oxygen species (ROS). The optimal degradation conditions were observed with 20 mg of catalyst applied to 5 mg/L of LVX at a neutral pH of 7.01, resulting in a 25.70% degradation rate after 120 minutes under low-intensity UV light. The primary ROS responsible for this degradation included hydroxyl radicals (•OH), superoxide radicals ($•O_2^-$), and photogenerated holes (h^+), which played crucial roles in the oxidative breakdown of LVX. A 20 mg catalyst dose offered the best balance, ensuring sufficient active sites without causing

light scattering. Degradation followed pseudo-first-order (PFO) kinetics, with lower LVX concentrations leading to faster rates due to enhanced interaction with the catalyst. Neutral pH conditions were most favourable for ROS generation and efficient catalyst-pollutant interactions. Gr's role in improving electron transfer and minimizing electron-hole recombination was key to the composite's performance. In addition to its photocatalytic performance, the ZIF-8/Gr exhibited antibacterial activity, as evidenced by an ZOI against E. coli under dark conditions. These findings suggest that ZIF-8/Gr is a promising material for wastewater treatment, offering both pollutant degradation under low light and antibacterial properties in the absence of light. Overall, the ZIF-8/Gr composite presents a sustainable, energy-efficient solution for the degradation of pharmaceutical pollutants in wastewater, showing promise for large-scale applications.

Keywords: photocatalyst; antibiotics; ZIF-8; graphene; reactive species

Abstrak tesis yang dikemukakan kepada senat Universiti Putra Malaysia sebagai memenuhi keperluan untuk Ijazah Sarjana Muda Sains dalam Kimia Perindustrian dengan Kepujian

Menilai Prestasi Fotokatalitik ZIF-8/Grafena Terhadap Levofloxacin

Oleh

CALVIN MANASSEH A/L MANIVEL

JANUARI 2025

Pengerusi : Alvin Lim Teik Zheng, PhD
Fakulti : Kemanusian, Pengurusan dan Sains

Kajian ini berjaya menunjukkan degradasi fotokatalitik levofloxacin (LVX) menggunakan komposit ZIF-8/grafena (Gr) di bawah penyinaran cahaya UV berkuasa rendah yang disimulasikan. Komposit ZIF-8/Gr mengatasi prestasi komponen individunya, mencapai kecekapan degradasi yang lebih tinggi dengan meningkatkan pemisahan cas, memperluas luas permukaan, dan meningkatkan penghasilan spesies oksigen reaktif (ROS). Keadaan degradasi optimum diperhatikan apabila 20 mg pemangkin digunakan ke atas 5 mg/L LVX pada pH neutral 7.01, menghasilkan kadar degradasi sebanyak 25.70% selepas 120 minit di bawah cahaya UV berintensiti rendah. ROS utama yang bertanggungjawab terhadap degradasi ini termasuk radikal hidroksil (•OH), radikal superoksida ($\bullet O_2^-$), dan lubang fotogenerasi (h^+), yang memainkan peranan penting dalam penguraian oksidatif LVX. Dos pemangkin sebanyak 20 mg menawarkan keseimbangan terbaik, memastikan tapak aktif mencukupi tanpa menyebabkan penyebaran cahaya. Degradasi mengikuti kinetik tertib pertama pseudo (PFO), di mana kepekatan LVX yang lebih rendah membawa kepada kadar yang lebih cepat akibat interaksi yang dipertingkatkan dengan pemangkin. Keadaan pH

neutral adalah paling sesuai untuk penjanaan ROS dan interaksi pemangkin-pencemar yang berkesan. Peranan Gr dalam meningkatkan pemindahan elektron dan meminimumkan rekombinasi elektron-lubang adalah kunci kepada prestasi komposit ini.Selain prestasi fotokatalitiknya, ZIF-8/Gr juga mempamerkan aktiviti antibakteria, seperti yang dibuktikan oleh zon perencatan (ZOI) terhadap E. coli dalam keadaan gelap. Penemuan ini mencadangkan bahawa ZIF-8/Gr adalah bahan yang berpotensi untuk rawatan air sisa, menawarkan keupayaan degradasi pencemar di bawah cahaya rendah serta sifat antibakteria dalam ketiadaan cahaya. Secara keseluruhannya, komposit ZIF-8/Gr mempersembahkan penyelesaian yang mampan dan cekap tenaga untuk degradasi pencemar farmaseutikal dalam air sisa, dengan potensi untuk aplikasi berskala besar.

Kata kunci: fotokatalis; antibiotik; ZIF-8; grafena; spesies reaktif

Graphical Abstract

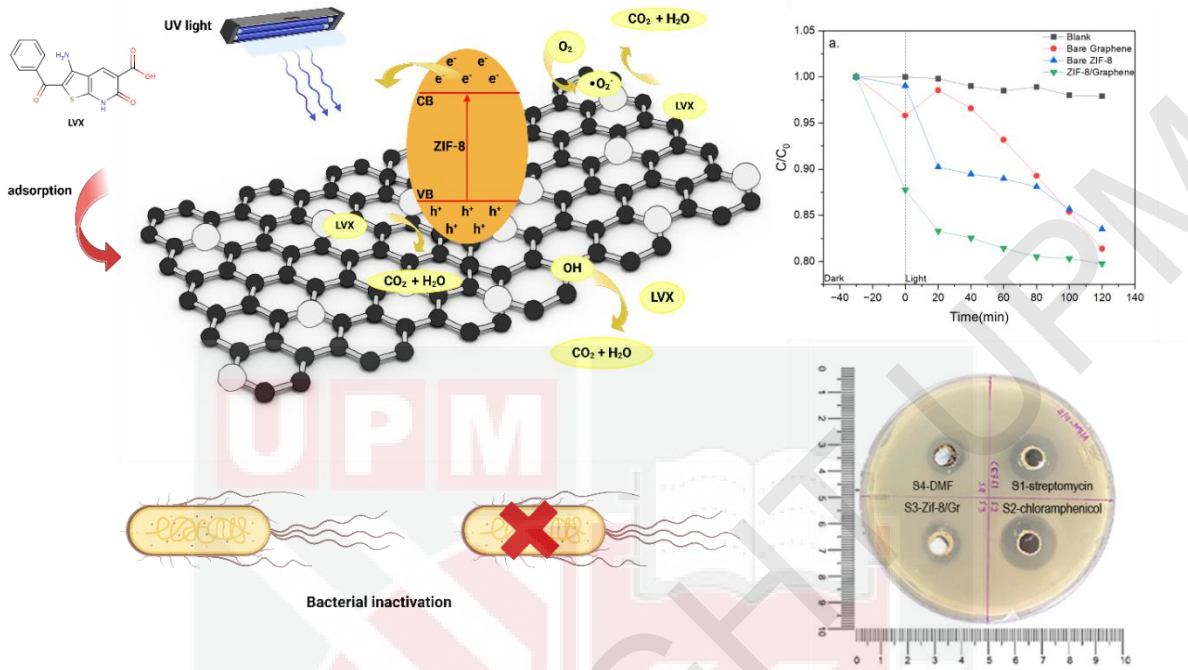

Highlights

- The ZIF-8/graphene (Gr) composite demonstrated enhanced photocatalytic degradation of levofloxacin (LVX) under low-intensity UV light compared to its individual components.
- Optimal conditions for LVX degradation, including a catalyst dose of 20 mg, a neutral pH of 7.01, and a low LVX concentration of 5 mg/L.
- ZIF-8/Gr composite exhibited antibacterial activity against E. coli under dark conditions
- The generation of ROS such as hydroxyl radicals (•OH), superoxide radicals ($\bullet O_2^-$), and photogenerated holes (h^+).

ACKNOWLEDGEMENT

First and foremost, I would like to express my deepest gratitude to the Almighty God for His endless blessings, guidance, and strength throughout this journey. His grace has granted me good health, perseverance, and wisdom, enabling me to complete this final year project successfully.

I extend my heartfelt appreciation to my supervisor, Dr. Alvin Lim Teik Zheng, for his invaluable guidance, unwavering support, and continuous encouragement throughout the entire research process. His insightful advice and constructive feedback have been instrumental in shaping this study and improving my understanding of the subject matter.

A special thank you to my final year project mates, Melissa and Thien, for their incredible support both mentally and academically. Their willingness to assist me during lab sessions, share knowledge, and provide motivation during challenging times has made this journey more manageable and enjoyable.

I am also deeply grateful to the laboratory assistants at UPM Bintulu for granting me access to the laboratory facilities and ensuring that I had everything needed to conduct my experiments smoothly. Additionally, I would like to extend my sincere thanks to the laboratory assistants at UPM Serdang, as well as Ms. Renuga, Praveen, and Chris for not only allowing me to utilize the lab but also for teaching me how to operate the necessary instruments and for their patience and company during lab sessions.

Lastly, I wish to express my profound gratitude to my family for their unwavering support in all aspects. Their financial assistance, mental and emotional encouragement, as well as constant prayers, have been my pillar of strength throughout this journey. Their belief in me has been a significant source of motivation, and I am forever thankful for their love and sacrifices.

ASSESSING THE PHOTOCATALYTIC PERFORMANCE OF ZIF-8/GRAPHENE TOWARDS LEVOFLOXACIN

BY

CALVIN MANASSEH A/L MANIVEL

S32695

APPROVED BY

Supervisor

_____ Date: 27 May 2025

(DR. ALVIN LIM TEIK ZHENG)

Project Coordinator

_____ Date: 27/05/2025

(DR. TENGKU SHARIFAH MARLIZA TENGKU AZMI)

TABLE OF CONTENTS

LIST OF FIGURES

LIST OF ABBREVIATIONS

CB	Conduction band
FTIR	Fourier transform infrared spectroscopy
GO	Graphene oxide
Gr	Graphene
LVX	Levofloxacin
MOF	Metal organic framework
rGO	Reduced graphene oxide
ROS	Reactive oxygen species
SEM	Scanning electron microscope
TGA	Thermogravimetric analysis
UV	Ultraviolet
VB	Valence band
XRD	X-ray diffraction
ZIF-8	Zeolitic-imidazolate framework

CHAPTER 1

INTRODUCTION

1.1 General Background

Water pollution is a widespread environmental problem caused by human activities, which leads to the contamination of various water bodies such as rivers, lakes, oceans, and groundwater. Contamination can stem from a range of sources, such as industrial discharges, agricultural runoff, sewage disposal, and improper waste management practices (Owa, 2014; Santika & W, 2021). The introduction of harmful substances into water systems has a detrimental impact on water quality and poses serious risks to both human health and ecosystems. It is alarming to note that water pollution-related diseases claim the lives of around 3.4 million people every year, as reported by the World Health Organization (WHO) (Tiwari et al., 2022).

The presence of antibiotics and other pharmaceuticals in water sources further complicates the relationship between water pollution and health. There has been a concerning rise in antibiotic-resistant bacteria due to the excessive and improper use of antibiotics in both agriculture and healthcare. This has resulted in the contamination of water systems, where these bacteria can thrive and multiply (Afroz & Rahman, 2017; Edokpayi et al., 2018). These resilient strains have the ability to infiltrate the human body via the ingestion of polluted water or food, resulting in infections that pose a growing challenge for treatment. Studies have shown that being exposed to these pollutants can disturb the delicate balance of the human microbiome, which may contribute to various health problems such as obesity, diabetes, and autoimmune diseases (Doğan et al., 2022; Jiang et al., 2022)

Levofloxacin (LVX) is a synthetic antibiotic that falls under the fluoroquinolone class. Table 1.1 depicts the chemical structure and properties of LVX. It is commonly used due to its effectiveness in treating various bacterial infections, such as respiratory tract infections, urinary tract infections, and skin infections. The mechanism of action involves the inhibition of

bacterial DNA gyrase and topoisomerase IV, which are crucial for bacterial DNA replication and transcription (Abukhadra et al.., 2020; Liu et al., 2021). LVX being a third-generation fluoroquinolone, is widely recognized for its ability to effectively combat a wide range of bacteria, including both Gram-positive and Gram-negative strains (Varma et al., 2022). LVX has a molecular formula of $C_{18}H_{20}FN_3O_4$ and a unique structure with a fluorine atom, which boosts its effectiveness against bacteria. The hydrophobic characteristics of the compound are attributed to the presence of the fluorine atom, enabling it to bind effectively to different environmental matrices, such as polystyrene nanoparticles (Arachchi et al., 2023). The stability of LVX in water is a matter of great concern. It has been observed that LVX can withstand degradation during conventional wastewater treatment processes, resulting in its long-lasting presence in aquatic environments. The stability of this compound is due to its unique chemical structure, which enables it to resist microbial and biological oxidation (Kumar et al., 2018; S. Zheng et al., 2022).

Table 1.1. The structure and properties of LVX

Chemical structure	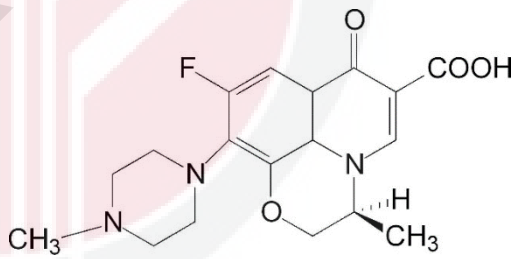
Chemical formula	$C_{18}H_{20}FN_3O_4$
Colour	White to pale yellow crystalline powder
pH value	4.5 to 6.5
Melting point	223-225 °C
Boiling point	400 °C

Stability	Stable under normal conditions but may degrade under extreme pH or temperature.
Solubility	Highly soluble in water and organic solvents such as methanol and ethanol.
Molecular weight (g/mol)	361.37 g/mol
Half-life	Approximately 6 to 8 hours in humans

(C. S. Han et al., 2023; Q. Wang et al., 2019)

Conventional wastewater treatment systems often fall short in effectively removing persistent antibiotics, leading to their accumulation in natural water sources. This inadequacy is primarily due to the limited efficiency of biological treatment processes, which fail to fully degrade antibiotic compounds, resulting in their discharge into the environment (A. Huangetal.,2021; Y. Liu et al., 2022; Oberoi et al., 2019).Consequently, the development of innovative wastewater treatment technologies is crucial. Among the most studied methods for enhancing antibiotic removal are adsorption, membrane filtration, advanced oxidation processes (AOPs), and photocatalysis, with the latter showing the greatest potential.

Adsorption is one of the most widely researched techniques for removing antibiotics from wastewater. In this method, antibiotic molecules adhere to solid surfaces, reducing their concentration in treated water. Activated carbon and various other adsorbents have been shown to improve the removal efficiency of antibiotics (Alvarino et al., 2018; Grandclément et al., 2017). However, the performance of adsorption is heavily influenced by several factors, such as the type of adsorbent used, the antibiotic concentration, and the presence of competing substances in the wastewater (J. Wang & Wang, 2018). These factors may limit the scalability and efficiency of adsorption in large-scale applications.

Membrane filtration is another effective strategy for separating antibiotics from wastewater. This process uses semi-permeable membranes to selectively allow water to pass through

while retaining antibiotic molecules. Membrane filtration has been shown to achieve high removal rates, although membrane fouling and the associated need for regular cleaning and maintenance pose practical challenges. To overcome these limitations, membrane filtration is often coupled with other methods, such as AOPs, to enhance overall treatment performance (Cincinelli et al., 2015; P. Liu et al., 2014)

AOPs are characterized by their ability to generate highly reactive radicals that oxidize and degrade organic pollutants, including antibiotics. Methods such as ozonation and UV irradiation have been shown to effectively break down antibiotic compounds in wastewater. Despite their effectiveness, AOPs can require significant energy inputs and may lead to the formation of harmful by-products, necessitating careful management of these systems. Consequently, while AOPs offer a robust method for pollutant degradation, their operational demands and potential side effects limit their widespread application (Chen et al., 2018; P. Liu et al., 2014).

Among the advanced treatment methods, photocatalysis stands out as the most promising technique for antibiotic removal from wastewater. Photocatalysis utilizes light-activated catalysts to degrade antibiotics and other organic pollutants into less harmful substances. Studies have demonstrated that photocatalytic processes can achieve high removal efficiencies, making them a viable option for sustainable wastewater treatment. Key advantages of photocatalysis include its operation under mild conditions, low energy consumption, and the absence of secondary pollutants, which make it highly attractive for large-scale applications. Additionally, advancements in photocatalytic materials, such as polyoxometalates, have further enhanced the performance and efficiency of these systems (Lan et al., 2021; J. Wu et al., 2022).

ZIF-8, a metal organic framework (MOF) is a highly promising semiconductor photocatalyst, especially in solar-driven applications, due to its many advantages. One key benefit is its effectiveness in breaking down various contaminants in water and air using semiconducting nanoparticles to create reactive oxygen species (ROS). Although ZIF-8 is widely utilized for

the photocatalytic degradation of organic pollutants, its stability in water and low photocatalytic activity remains significant limitations due to poor adsorption efficiency and challenges associated with the migration and separation of electron-hole pairs (X. Han et al., 2023; Senapati et al., 2024). The stability issue arises from the tendency of ZIF-8 particles to agglomerate in water, which can hinder their effectiveness in practical applications (X. Han et al., 2023). Furthermore, the wide band gap of ZIF-8, approximately 4.9 eV, limits its responsiveness to visible light, necessitating the use of UV light for activation, which is not always feasible in natural settings (Senapati et al., 2024). This limitation is compounded by the fact that the photogenerated electron-hole pairs can recombine before participating in the degradation process, thereby reducing the overall efficiency of the photocatalytic reaction (R. Guo et al., 2021). Therefore, there is a need to develop more efficient photocatalysts that can degrade antibiotic pollutants. ZIF-8, with its unique visible light harvesting properties and compatibility with graphene (Gr), has the potential to address these challenges. However, its application in LVX degradation remains underexplored. This study seeks to fill this gap by fabricating a ZIF-8/Gr and evaluating its photocatalytic performance.

1.2 Problem statement

The increasing presence of antibiotic pollutants like LVX in aquatic environments presents a significant threat to both ecosystems and public health, exacerbated by the limitations of conventional wastewater treatment methods in effectively breaking down these emerging contaminants. This study addresses the urgent need for innovative and efficient approaches to LVX degradation by exploring the photocatalytic potential of a ZIF-8/Gr composite catalyst. Despite the promising advantages of the ZIF-8/Gr composite, the understanding of its photocatalytic mechanisms, optimal synthesis conditions, and performance under real-world conditions remains limited. To address these gaps, this study systematically investigates the photocatalytic efficiency of the ZIF-8/Gr composite in degrading (LVX). By exploring the composite's behaviour in this context, the research aims to advance the development of more efficient and sustainable remediation technologies for environmental applications.

In addition, despite the effectiveness of photocatalysis under high-intensity light sources, the challenge of utilizing low-intensity light for such applications remains underexplored. In this research, we synthesized the ZIF-8/Gr composite via a hydrothermal method and characterized its structure, morphology, and thermal stability. Under low-intensity light irradiation, the composite demonstrated significant improvements in LVX degradation compared to ZIF-8 alone, driven by enhanced charge separation and increased production of ROS. This work highlights the promising role of ZIF-8/Gr composites in advancing sustainable wastewater treatment, even under suboptimal lighting conditions, offering a powerful solution to the pressing issue of antibiotic pollution.

1.3 Objectives

The primary goal of this thesis is to synthesize ZIF-8/Gr composite using the environmentally friendly hydrothermal method. In addition, the study examines the physical and chemical properties of the photocatalyst and evaluates its effectiveness in LVX photodegradation under low intensity UV light source. Several characterization techniques were employed to analyse the composite. To accomplish this, four key research objectives were identified and pursued as outlined below:

i. To synthesize ZIF-8/Gr using the green hydrothermal method.
ii. To characterize ZIF-8/Gr using XRD, FTIR, SEM, and TGA.
iii. To assess the photocatalytic performance of ZIF-8/Gr towards LVX and their antibacterial/antioxidant properties.
iv. To predict the photodegradation mechanism of LVX.

CHAPTER 2

LITERATURE REVIEW

2.1 Photocatalysis and degradation mechanism

Photocatalysts are materials that speed up chemical reactions when exposed to light, usually by producing ROS that can assist in different chemical transformations. Photocatalysis is based on the absorption of photons, which leads to the excitation of electrons from the valence band (VB) to the conduction band (CB), resulting in the formation of electron-hole pairs. The charge carriers can actively engage in redox reactions, resulting in the breakdown of pollutants, generation of hydrogen, or other chemical processes (Mu et al., 2024). The effectiveness of a photocatalyst is typically assessed by its capacity to absorb light, the duration of the excited states, and the movement of the charge carriers (X. Zeng et al., 2016). For instance, titanium dioxide (TiO_2), zinc oxide (ZnO), bismuth vanadate ($BiVO_4$), and among others has been extensively researched as a photocatalyst because of its exceptional efficiency and stability when exposed to light.

The photodegradation mechanism is depicted in Fig. 2.1. Electron-hole pairs are created when the photocatalyst absorbs photons with energy equal to or higher than its bandgap energy. This process involves moving part of the electrons from the VB to the CB. When light is absorbed, the photocatalyst produces electron-hole pairs. Positively charged holes (h^+) are left behind in the VB as electrons are stimulated from the VB to the CB. These highly reactive electron-hole pairs are crucial for initiating chemical reactions on the surface of the photocatalyst. Organic pollutants from water adsorb onto the surface of the photocatalyst due to weak physical interactions, such as van der Waals forces or electrostatic attractions, from the surrounding environment. Once adsorbed onto the photocatalyst surface, the organic molecules will encounter the generated electron-hole pairs. The excited electrons (e^-) in the CB can directly reduce the organic pollutants by transferring their energy to them, breaking chemical bonds and generating radical species. Meanwhile, the h^+ in the VB can oxidize water

molecules or hydroxide ions (OH^-) present in the surrounding medium, producing hydroxyl radicals (•OH), which are highly reactive oxidizing species. By means of chemical bond cleavage, hydroxylation, or dichlorination, the organic pollutants are attacked by the produced radicals. Until the organic molecules are fully mineralized into carbon dioxide, water, and basic inorganic ions, this breakdown process is continued. The photocatalyst itself is not consumed by the photocatalytic process, meaning that it can be recycled for more degradation cycles.

Previously, it was found that photocatalyst such as TiO_2 can be effectively reused, maintaining their photocatalytic activity over extended periods (Jafri et al., 2022; T. Zhang et al., 2014). The continuous process of using photocatalysts is dependent on the presence of light energy. The photocatalytic activity can continue for as long as there is enough light exposure, gradually eliminating organic pollutants from the environment.

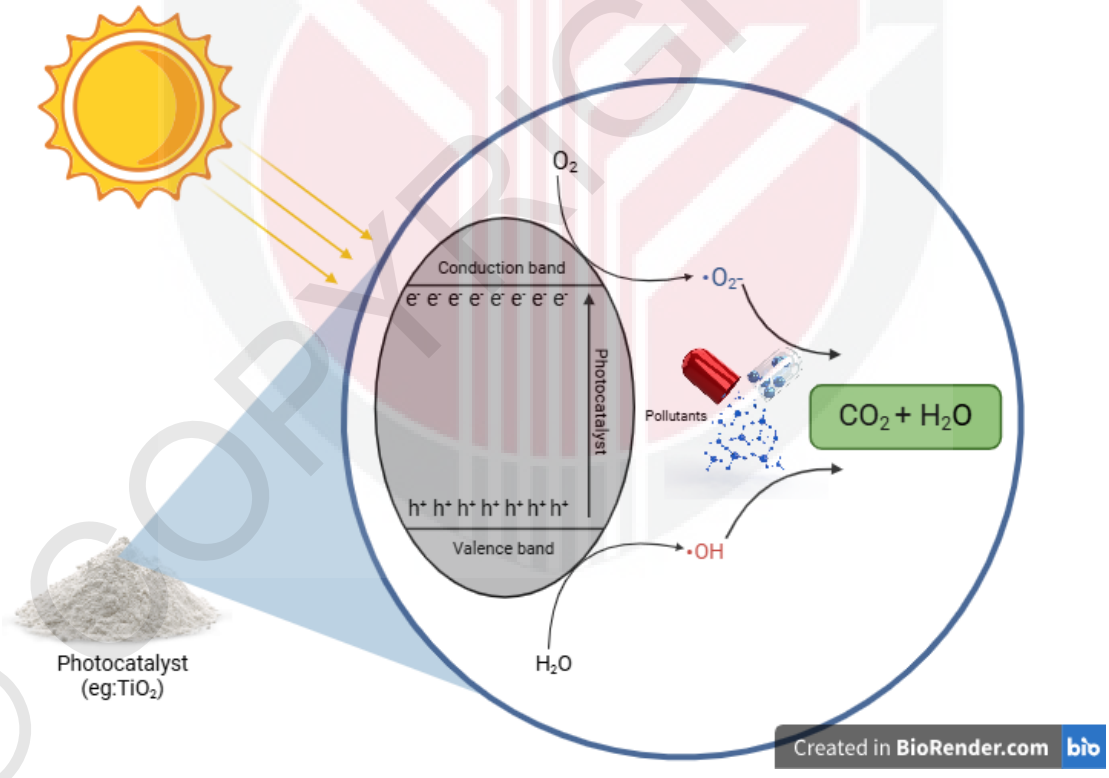

Fig. 2.1. Schematic of photocatalytic degradation mechanism of pollutants.

There have been recent developments in the field of photocatalysis, specifically in the use of visible light-active photocatalysts. These photocatalysts, including doped semiconductors and other composite materials, have shown promising results in improving the efficiency of photocatalytic reactions when exposed to sunlight (Alansi et al., 2021; Zou et al., 2021). Several factors can affect the efficiency of degradation, such as the choice of photocatalyst, the concentration of pollutants, and the surrounding environmental conditions like pH (Bobirică et al., 2021; Paliwal & Shorgar, 2023).

2.2 ZIF-8 as a photocatalyst

Photocatalysts made from MOFs have attracted a lot of interest because of their distinct structural features. These features include a large surface area, customizable porosity, and the ability to incorporate different metal ions and organic linkers. Guest molecules can be accommodated within MOFs due to their porous nature. This unique structural property can have a positive impact on photocatalytic activity by either creating more reactive sites or aiding in charge transfer processes (Nguyen, 2021; L. Zeng et al., 2016). In addition, the flexibility of MOFs allows for adjustments to their electronic properties, resulting in improved light absorption and enhanced photocatalytic performance (Saliba et al., 2018).

The synthesis of ZIF-8 using the co-precipitation method is recognized as a straightforward and efficient approach that has been extensively explored for various applications. This method involves the simultaneous precipitation of metal ions, specifically Zn ions, and organic linkers, such as 2-methylimidazole (MeIM), to form the ZIF-8 structure. The co-precipitation technique is advantageous due to its simplicity, cost-effectiveness, and ability to produce ZIF-8 with desirable properties tailored for specific applications. For instance, Pang et al. demonstrated that the controlled synthesis of ZIF-8 through co-precipitation allowed for the formation of nanocomposites with enhanced functionalities, such as magnetically separable nano catalysts. Similarly, Ma and co-workers highlighted the synthesis of ZIF-8@TiO_2 nanoribbon catalysts using ultrasonication, which further illustrates the versatility of the co-

precipitation method in producing composite materials with improved catalytic activity (Ma et al., 2023; Pang et al., 2015).

The presence of certain metal ions, such as copper, can significantly accelerate the formation of ZIF-8 crystals. These metal ions act as modulators in the reaction, influencing the morphology and growth of ZIF-8. For instance, ZnAl-CLDH/ZIF-8 composites were created using co-precipitation, which enhanced the photocatalytic degradation of organic dyes such as methyl blue (Y. Wang et al., 2021).

The potential of ZIF-8 in this thesis is highlighted by its proven photocatalytic properties and its capacity to improve the performance of other photocatalysts. ZIF-8 possesses unique structural characteristics and can be easily functionalized, making it a highly promising option for the creation of cutting-edge photocatalytic systems that can contribute to sustainable energy solutions and environmental remediation. In addition, the potential to enhance ZIF-8's optical properties through doping or composite formation makes it an intriguing area of investigation in this study. Continued investigation into ZIF-8 and its composites will play a vital role in advancing the development of highly effective photocatalytic materials.

2.3 Composite derived from ZIF-8

Previous studies have shown that ZIF-8 based composites have great potential in the photocatalytic degradation of organic pollutants. The strength of these composites lies in their enhanced photocatalytic efficiency, which can be improved through the introduction of various substances that modify their properties. For example, the incorporation of carbon-based materials like reduced graphene oxide (rGO) or metal oxides such as TiO_2 which enhances light absorption and charge separation, leading to better photocatalytic performance (He et al., 2020). For example, the Ag@ZIF-8/g-C_3N_4 composite demonstrated improved degradation of antibiotics under visible light, showcasing the effectiveness of integrating ZIF-8 with other materials (Guo et al., 2022). Furthermore, ZIF-8/TiO_2 composites have shown significant improvements in degrading organic pollutants like Rhodamine B due to the

synergistic effects between the materials, enhancing light absorption and charge separation (Jeon et al., 2021; W. L. Zhong et al., 2024).

One key advantage of the inclusion of ZIF-8 in composites is their ability to alter the band gap, which is crucial for photocatalytic activity. For instance, combining ZIF-8 with Bi_2MoO_6 forms a heterojunction that facilitates the transfer of photogenerated charge carriers, improving photocatalytic activity under visible light (Xia et al., 2019). Additionally, integrating noble metals like silver (Ag) into ZIF-8 enhances its light-harvesting capabilities due to plasmonic effects, promoting better separation of electron-hole pairs, which is crucial for efficient pollutant degradation. Despite these strengths, ZIF-8 composites face challenges, particularly in terms of durability under operational conditions. ZIF-8 can experience structural degradation in humid environments or after prolonged exposure to light, which reduces its photocatalytic efficiency (Bhattacharyya et al., 2020).

2.4 Graphene-based composite photocatalyst

Gr is an extremely thin film of carbon atoms that form a distinctive honeycomb pattern. It possesses extraordinary qualities such as outstanding electrical and thermal conductivity, impressive mechanical strength, and remarkable flexibility. The distinctive arrangement of carbon atoms in Gr, with sp^2 hybridization, enhances electron mobility, which has led to its potential use in a wide range of applications such as electronics, sensors, and catalysis (Novoselov et al., 2012; Sanchez et al., 2012).

Gr possesses remarkable electrical conductivity, showcasing exceptional intrinsic carrier mobility that surpasses that of conventional semiconductors (Fukidome et al., 2014). This unique characteristic makes it an ideal material for high-speed electronic devices. When it comes to mechanical strength, Gr boasts an impressive Young's modulus of around 1 TPa and a remarkable tensile strength exceeding 130 GPa. This places it among the elite group of the strongest materials known to us (Khan et al., 2017), offering great potential for reinforcing composite materials and significantly improving their durability. The chemical reactivity of Gr

is also important, as its surface can be modified to improve its compatibility with other materials. This has led to the creation of a plethora of hybrid composites (Kodali et al., 2011).

One previous study has shown that when semiconductors such as ZnO is incorporated with Gr; the photocatalytic performance improved significantly. Yang and colleagues found that he the incorporation of rGO caused a slight red shift in the absorption peak, enhancing the visible-light absorption capability of the composites (X. Yang et al., 2021)

Enhanced charge separation is observed as Gr facilitates electron transfer between ZIF-8 and the substrate, resulting in reduced charge recombination and increased photocatalytic efficiency. This is a critical aspect in the degradation of pollutants, as highlighted by previous studies (Autreto et al., 2014; Y. Liu et al., 2012). Another benefit is the increased stability that comes with using Gr. This enhanced the mechanical and thermal resilience of ZIF-8 composites, allowing for sustained catalytic activity even under operational (Chemello et al., 2023; Khan et al., 2017; Novoselov et al., 2012). Previous studies have found that the combination of Gr and ZIF-8 leads to a higher number of active sites for catalytic reactions, resulting in a significant boost in overall catalytic activity. Finally, the combination of Gr led to synergistic effects that enhanced reactant adsorption and accelerated reaction kinetics, resulting in enhanced catalytic performance (Autreto et al., 2014; Y. Liu et al., 2012).

2.5 Hydrothermal method

The hydrothermal method is a widely recognized synthesis technique used for the crystallization of substances from high-temperature aqueous solutions under controlled pressure. This method utilizes the distinct characteristics of water as a solvent, specifically its heightened capacity to dissolve various substances under high temperatures and pressures. Under these specific conditions, the solubility of reactants is greatly enhanced, leading to the creation of crystalline products with precisely controlled properties. The process is usually carried out in a sealed vessel called an autoclave, where temperature and pressure are carefully controlled to promote crystal growth and the development of nanostructures (P. Wang

et al., 2023). One major benefit of the hydrothermal method is its ability to produce materials with precise shapes and sizes, which is essential for applications in catalysis, electronics, and energy storage. Previous study has reported the integration of Gr, particularly rGO, into MOFs is achieved by mixing graphene oxide (GO) with metal precursors and ligands in a hydrothermal setup. This process not only reduces GO but also facilitates the formation of a composite material with enhanced properties (Saha et al., 2014). For example, Fe_3O_4/rGO composites prepared cia hydrothermal method demonstrated excellent electrochemical performance, while α-Fe_2O_3–rGO composites show high adsorption capacity for dye removal from water (A. Liu et al., 2015).

2.6 Photocatalytic degradation performance of MOF/Gr composite.

Table 2.1 described some selected photocatalytic performance of Gr based composites photocatalysts towards the degradation of various pollutants.

Heu and colleagues investigated the performance of UiO-66/GO composite synthesized via hydrothermal method for the degradation of carbamazepine, a common pharmaceutical contaminant in wastewater (Heu et al., 2020). Their study revealed that the photocatalyst demonstrated a remarkable degradation efficiency of 90%, primarily facilitated by superoxide radicals ($\bullet O_2^-$) and hydroxyl radicals (•OH). These reactive species play crucial roles in the oxidative breakdown of carbamazepine, effectively breaking down the molecular structure of the pollutant. The study also emphasized that the enhanced photocatalytic activity was attributed to the synergistic effect between the MOF and GO, which improved charge carrier separation and light absorption, resulting in a more efficient photocatalytic process.

Similarly, Yang and colleagues explored the performance of MIL-68(In)-NH_2/GO composite, prepared using a solvothermal method for the degradation of amoxicillin, another widely used antibiotic (C. Yang et al., 2017). Their prepared catalyst achieved an impressive degradation efficiency of 93%, leveraging •OH and $\bullet O_2^-$ to effectively decompose the antibiotic. Their study highlighted the importance of the amine functional groups in MIL-68, which not only improved

the adsorption of amoxicillin but also facilitated the generation of reactive species under light irradiation. Hence, the incorporation of GO into the composite not only enhanced the charge transfer between the components but also significantly increased the surface area, allowing for more active sites for pollutant adsorption and subsequent degradation.

Bouider and colleagues reported on the synthesis of MOF-5/GO using a modified Hummer's method, targeting the degradation of methylene blue (Bouider et al., 2023). The results indicated a degradation efficiency of 92%, attributed to the involvement of $\bullet O_2^-$, •OOH, and •OH during the photocatalytic process. Their study provided insights into the mechanism, showing that the presence of GO facilitated the generation and stabilization of these reactive species, leading to effective dye degradation. Additionally, the research underscored the importance of optimizing the GO content to balance light absorption and the availability of active sites, which directly impacts the photocatalytic performance of the composite.

Furthermore, Wu and his co-workers introduced a novel MIL-88(Fe)/GO composite, synthesized through a facile and rapid single-step (modified hummers method) demonstrating its effectiveness in degrading both methylene blue and rhodamine B under sunlight (Y. Wu et al., 2014). Their synthesized catalyst achieved a remarkable degradation efficiency of 100%, with •OH identified as the main oxidative species responsible for the dye degradation. The study elaborated on the structural characteristics of MIL-88, which provided a robust framework for the immobilization of GO, thus enhancing the overall stability and reusability of the photocatalyst. Overall, previous studies on MOF/Gr contributes significantly to the understanding of how to leverage advanced materials for effective pollutant degradation in real-world scenarios.

Table 2.1 Selected photocatalytic performance of Gr composited photocatalysts towards the degradation of pollutants.

No	BCPs	Synthesis Method	Pollutant	Degradation efficiency (%)	ROS involved	Reference
1	MIL-68(In)-NH_2/GO	Solvothermal	Amoxicillin	93%	•OH, $•O_2^-$	(C. Yang et al., 2017)
2	MOF-5/GO	Modified Hummer's method	Methylene blue	92%	$•O_2^-$, •OOH, h^+, •OH	(Bouider et al., 2023)
3	NH_2-MIL-125/rGO	Solvothermal	Methylene blue	96.70%	•OOH	(L. Huang & Liu, 2016)
4	MIL-88(Fe)/GO	Hydrothermal	Methylene blue and Rhodamine B	100%(sunlight)	•OH	(N. Liu et al., 2018)
5	UiO-66/GO	Hydrothermal	Carbamazepine	90%	$•O_2^-$, •OH	(Heu et al., 2018)
6	Ag_2CO_3/Gr	Precipitation	Methyl orange	95%	•OH	(Chen et al., 2018)
7	ZnO/Gr	Solvothermal	Congo red	71.97%(6%rGO)	•OH	(Atchudan et al., 2017)
8	$BiWO_6$/Gr	Hydrothermal	Methylene blue	88.10%	$•O_2^-$, h^+	(Zhou & Zhu, 2012)

9	$SrTiO_3$/Gr	Photocatalytic reduction of GrO	Acid orange	88%	•OH, h^+, •OOH	(Xian, Yang, Di, et al., 2014)
10	LSMO/Gr	Mixing and thermal drying	Methyl red	53%	•OH, h^+	(Xian, Yang, Wang, et al., 2014)
11	$BiVO_4$/Gr	Ultrasonication	Rhodamine B	87%	•OH, $•O_2^-$	(Xu et al., 2014)
12	MIL-125/Biochar	One-step hydrothermal	Tetracycline hydrochloride	94.62%	h^+, $•O_2^-$	(Z. Liu et al., 2022)
13	ZIF-8	Slow evaporation	Methylene blue	82.30%	•OH	(Z. Liu et al., 2022)
14	rGO/TiO_2	Electrophoretic deposition	4-chlorophenol	70%	•OH	(Zouzelka et al., 2019)
15	Gr/TIO_2/Fe_3O_4	Mixing and evaporation	Phenol	96.9%	•OH	(Heltina et al., 2022)

CHAPTER 3

METHODOLOGY

3.1 Materials

2-methylimidazole (Macklin, China), methanol (HmBG, Malaysia), zinc nitrate hexahydrate ($Zn(NO_3)_2 \cdot 6H_2O$, (Sigma-Aldrich), and graphene oxide (GO) suspension (Nippon Shokubai, Japan) were purchased for use in this study. Hydrochloric acid (HCl, Sigma-Aldrich), sodium hydroxide (NaOH, Sigma-Aldrich), and levofloxacin (Tokyo Chemical Industry, TCI, Japan) were also obtained. All chemicals were of analytical grade and used without further purification. Solutions were prepared in deionized water (pH 6.5 – 7) throughout the experiments.

3.2 Synthesis of ZIF-8

Nanoscale ZIF-8 is synthesized using the co-precipitation method as shown in Fig. 3.1.(a). This method involves the simultaneous precipitation of zinc ions and organic linkers, typically 2-methylimidazole, leading to the formation of ZIF-8 crystals. The co-precipitation technique is favoured for its simplicity and efficiency, enabling the production of ZIF-8 with desirable properties for various applications (Chin et al., 2018). In a typical synthesis method, 1.78 g of Zn (NO3)2·6H2O and 5.26 g of 2-methylimidazole were dispersed in two separate beakers containing 40 ml of methanol each. The suspension was then stirred at room temperature for 6 h. The product was recovered by centrifugation and washed three times with fresh methanol. It was then dried at 80 °C for 12 h, followed by activation in a vacuum oven for an additional 12 h.

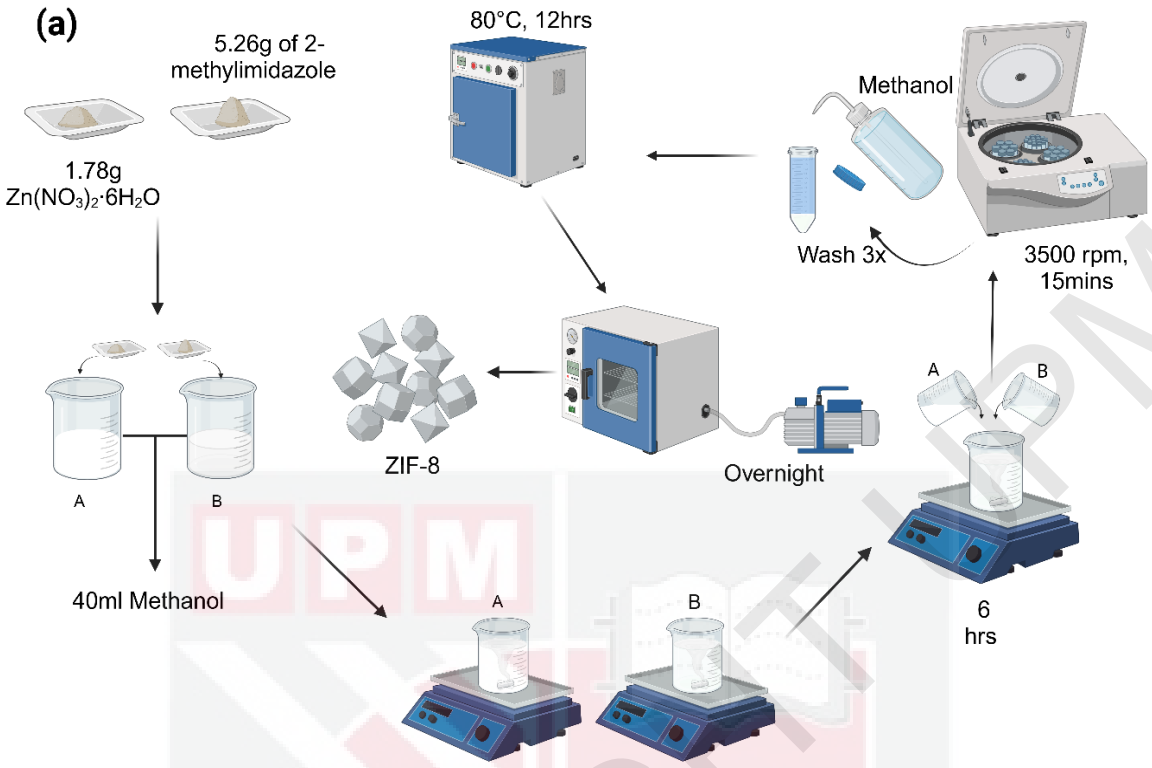

Fig. 3.1. Synthesis of ZIF-8.

3.3 Synthesis of ZIF-8/Gr

The synthesis of ZIF-8/Gr was achieved using the hydrothermal method as shown in Fig. 3.2. (b). First, 9 g of GO was dispersed in deionized water and sonicated for 3–5 hours, ensuring complete dispersion. Following this, 30 mg of as-synthesized ZIF-8 was added to the GO suspension, and the mixture was stirred at 400 rpm for 1 hour using a magnetic stirrer. The resulting mixture was then transferred into a 200 mL Teflon-lined autoclave and subjected to hydrothermal treatment at 180°C for 18 hours. After cooling to room temperature, the ZIF-8/Gr suspension was filtered via vacuum filtration and thoroughly washed with ethanol and distilled water to remove any residual impurities. The filtered product was dried in an oven at 80°C for 12 hours. Finally, the dried composite was carefully collected, ground into a fine powder, and stored for further characterization and analysis.

Fig. 3.2. Synthesis of ZIF-8/Gr.

3.4 Characterization

3.4.1 Chemical characterization – FTIR

Fourier Transform Infrared (FT-IR) spectroscopy was conducted to analyse the chemical structure of the ZIF-8/Gr composite using a Agilent Cary 630 FTIR spectrometer (Agilent Technologies, USA). The ZIF-8/Gr powdered sample was prepared using the KBr pellet method. Approximately 1 mg of the composite powder was mixed with 100 mg of spectroscopic-grade potassium bromide (KBr) and finely ground in an agate mortar to achieve a homogeneous mixture. The mixture was then transferred into a pellet die and compressed under a pressure of 3.5 tons for 15 seconds to form a transparent pellet. FT-IR spectra were recorded in the range of 4000–400 cm^{-1} at a resolution of 4 cm^{-1}, with 32 scans averaged for each measurement to improve the signal-to-noise ratio. A background spectrum was obtained using a blank KBr pellet and subtracted from the sample spectrum to account for any KBr

matrix interference. The resulting spectra were analysed to identify functional groups and confirm the successful incorporation of ZIF-8 into the Gr matrix.

3.4.2 Structural characterization – XRD

Powder X-ray diffraction analysis (XRD) was conducted to characterize the crystallography of bare ZIF-8 and ZIF-8/Gr. XRD serves as a powerful analytical non-destructive technique, allowing for the determination of crystal structure, size, and material strain through the analysis of diffraction patterns generated. The samples were finely ground to ensure a uniform particle size and placed in an XRD sample tray, with care taken to achieve even distribution and a flat surface to minimize errors in the diffraction data caused by variations in sample thickness. The analysis was performed using a Shimadzu model XRD6000 Power X-ray diffractometer at the Faculty of Science, UPM, utilizing CuKα radiation with a maximum voltage of 60 kV and a current of 60 mA. The scanning range was set from 2θ = 2° to 80°, with a step size of 0.02°/s. The crystallite size corresponding to each diffraction peak was calculated using Scherrer's formula:

$$D = k\lambda/\beta cos\theta$$

where D represents the crystallite size, k=0.89 is the Scherrer constant, λ wavelength (λ) of the Cu-radiation was 1.54056 Å for CuKα$_1$ radiation, and β is the half-peak width.

3.4.3 Morphological characterization – SEM

The JCM-6000 Versatile Benchtop Scanning Electron Microscope (SEM) manufactured by JEOL Ltd (Japan) was utilized to investigate the surface morphology of bare ZIF-8 and ZIF-8/Gr. This high-resolution imaging provided valuable insights into the morphology and distribution of the components within the synthesized materials. To improve the electrical conductivity of the samples, a thin carbon coating was applied to the surface using a HITACHI E-1045 ion sputtering meter for a duration of 1 minute prior to examination. The SEM analysis was performed at an acceleration voltage of 15 kV and a magnification of 500 times, enabling detailed observation of the surface features and structural characteristics of the catalysts.

3.4.4 Thermal characterization – TGA

Thermogravimetric and differential thermal analysis (TGA/DTA) of the catalysts was conducted using a Mettler Toledo thermogravimetric analyser. TGA measures the mass change of a material as a function of temperature and time under controlled atmospheric conditions. This analysis primarily aimed to assess the thermal stability of the synthesized catalysts. The thermal stability tests were performed in a nitrogen atmosphere, with a nitrogen flow rate of 100 mL/min and a heating rate of 10 °C/min, covering a temperature range from 35 °C to 800 °C. This comprehensive thermal analysis provides valuable insights into the stability and performance of the catalysts

3.4.5 Optical characterization

The optical properties of ZIF-8/Gr were analysed using UV–vis absorption spectrophotometer SCINCO UV-Visible Spectrophotometer model no.(S-3100). The Tauc plot is commonly used to estimate the optical band gap energy of a semiconductor material. The band gap energy (E_g) is an important parameter, as it dictates the range of light wavelengths that a semiconductor can absorb, making it crucial for applications like photovoltaics, photocatalysis, and optoelectronics. The band gap of ZIF-8/Gr, was calculated by formula below:

$$(\alpha h\nu)^2 = A\,(h\nu - E_g)$$

where α, h, v, A and E_g denoted the absorption coefficient, Planck constant, frequency of light, constant and band gap, respectively.

3.5 Photodegradation of LVX

This study investigates the photocatalytic performance of bare ZIF-8 and ZIF-8/Gr composites by examining the degradation of LVX under simulated visible light irradiation. The photocatalytic reactions were carried out in a custom-designed wooden chamber using an Aquarium UV-Sterilizer Lamp (13W52) as the light source. Prior to photo-illumination, the system was maintained in the dark for 30 minutes to evaluate the contribution of the adsorption process.

The photodegradation experiments were conducted in 100 mL aqueous LVX solutions, with a catalyst dosage of 100 mg of either bare ZIF-8 or ZIF-8/Gr composite. Samples were illuminated, and 3.5 mL aliquots were collected at regular intervals to monitor the degradation process. The concentration of LVX in each sample was determined using an iKEMELAB UV1200 UV-Vis spectrophotometer (China), which operates in the wavelength range of 320-1020 nm. The maximum absorbance wavelength (λ_{max}) for LVX was set at 290 nm. The degradation efficiency was calculated using the following formula:

$$\text{Degradation efficiency} = \frac{(C_0 - C_t)}{C_0} \text{x} 100\%$$

where C_0 represents the initial concentration of LVX, and C_t denotes the concentration of the pollutant after irradiation at time, t minutes.

3.6 Optimization studies

3.6.1 Influence of LVX concentration

For this experiment, various concentrations of 100 mL LVX were prepared at 5, 10, and 20 mg/L to assess the photocatalytic performance of the synthesized ZIF-8/Gr composite. The photodegradation experiments were carried out in 100 mL of various concentration of LVX (10, 20 and 50 mg/L) aqueous solutions. A sample of 10mg of the ZIF-8/Gr was then added to each solution. After the dark adsorption period, the solutions were illuminated with simulated visible light to initiate the photocatalytic degradation process. The data gathered from these experiments will provide insights into the optimal LVX concentration for efficient photocatalytic degradation.

3.6.2 Influence of pH

For this experiment, aqueous solutions of 100 mL, 5 mg/L LVX were prepared at pH values of 4, 7 and 9, adjusted using 0.1 M sodium hydroxide (NaOH) and hydrochloric acid (HCl). A sample of 10 mg of the ZIF-8/Gr was then added to each solution. The photodegradation experiments were conducted at a specified pH level. The data obtained from these

experiments will contribute to a deeper understanding of the photodegradation process under varying pH conditions.

3.6.3 Influence of amount of catalyst

For this experiment, the influence of the amount of catalyst on the photodegradation of LVX was investigated using varying quantities of the ZIF-8/Gr composite. A series of experiments were conducted with catalyst amounts of 5 mg, 10 mg, and 20 mg, each added to approximately 100 mL of the LVX solution at a constant concentration of 5 mg/L. The data gathered from these experiments will provide insights into the optimal catalyst dosage required for efficient photocatalytic degradation.

3.6.4 Radical trapping test

For this experiment, a radical trapping test was conducted to identify the reactive species involved in the photocatalytic degradation of LVX using the ZIF-8/Gr composite. Four sets of experiments were performed, each using different radical scavengers to capture specific ROS. Methanol was used to capture hydroxyl radicals (•OH), tert-butanol and ascorbic acid to capture superoxide radicals ($\bullet O_2^-$), and ethylenediaminetetraacetic acid (EDTA) to capture photogenerated holes (h^+). In each set, 100 mg of the ZIF-8/Gr was added to 100 mL of the LVX solution (5 mg/L), followed by the addition of 4 – 5 drops of 10 mM of the respective scavengers. The findings provided insights into the key reactive species involved in the photocatalytic mechanism.

3.7 Antibacterial test

The disk diffusion method was employed to evaluate the antibacterial activity of the prepared ZIF-8/Gr composite. Gram-positive *Staphylococcus aureus* and Gram-negative *Escherichia coli* bacteria were grown in Luria Bertania (LB) broth at 37 °C overnight. The bacterial suspensions were inoculated on Mueller-Hinton agar plates at a density of 1.5×10^6 CFU/mL and adjusted to a turbidity of 0.5 McFarland standard. Sterile filter discs (6 mm in diameter) impregnated with 1mg/mL of ZIF-8/Gr suspensions, dissolved in DMF as the solvent, were

prepared separately. Standard susceptibility discs soaked in streptomycin (30 µg) and chloramphenicol (30 µg) were used as positive controls, while discs soaked in sterile deionized water served as the negative control. Four sample holes were made on the agar plates to dispense the suspension of ZIF-8/Gr, streptomycin, chloramphenicol and deionized water. The filter paper discs were placed on top of the Mueller-Hinton agar plates, which were then incubated at 37 °C for 24 hours. The antibacterial activity of the ZIF-8/Gr was evaluated by measuring the zone of inhibition (ZOI) (mm) using a Vernier calliper. All plates. All experiments were carried out in triplicate and data were expressed as mean ± standard deviation (SD).

3.8 Antioxidant test.

The antioxidant activity of the ZIF-8/Gr was evaluated using the DPPH (2,2-diphenyl 1-picrylhydrazyl) radical scavenging assay. The test is crucial for determining the material's ability to neutralize harmful free radicals, a key factor in potential environmental applications. The ZIF-8/Gr was dissolved in two different solvents—dimethylformamide (DMF), and methanol to assess how solvent choice influences antioxidant activity. For the DPPH assay, a 1.9 mM solution of DPPH in methanol was prepared, and 0.1 mL of each ZIF-8/Gr solution was added to 2 mL of DPPH solution. The mixtures were incubated in the dark at room temperature for 30 minutes to avoid light interference. The colour change is determined by measuring absorbance with a spectrophotometer at 517 nm.

CHAPTER 4

DISCUSSION

4.1 FTIR Characterization

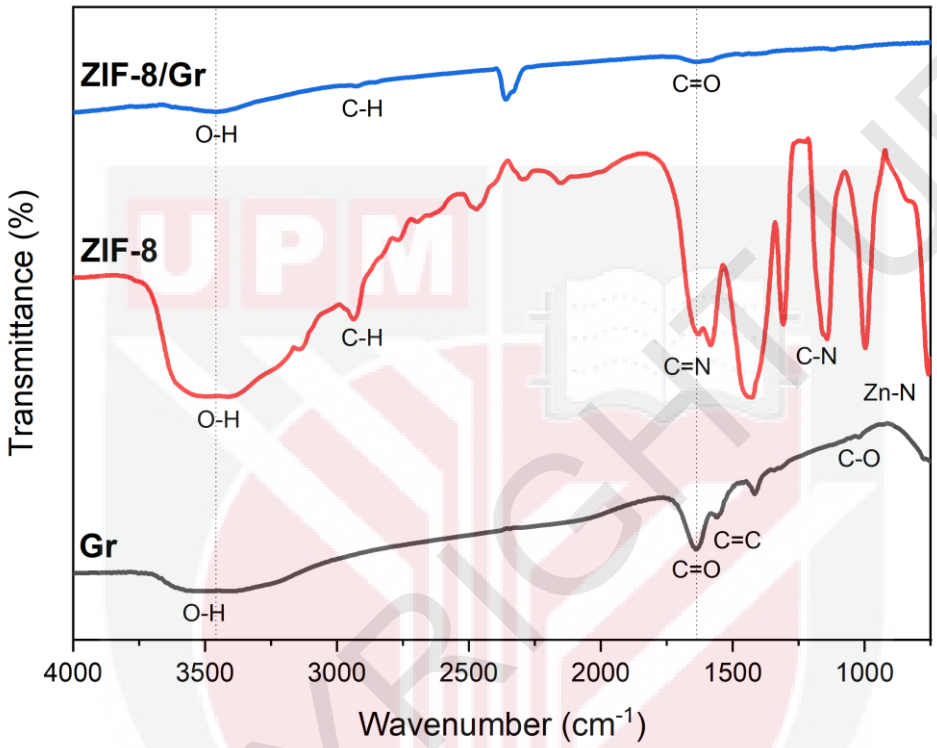

Fig. 4.1. FTIR of bare ZIF-8, Gr and ZIF-8/Gr.

The FTIR spectrum of bare ZIF-8 depicted in Fig. 4.1, reveal distinct vibrational bands characteristic of its structure. Prominent peaks between 900–1500 cm^{-1} correspond to the C–N stretching and bending vibrations from the imidazole rings that form the ZIF-8 framework. The sharp bands at 995 and 1142 cm^{-1} correspond to the characteristic stretching vibrations of the C–N bond in the imidazole ring, while the peaks at 1307 and 1145 cm^{-1} are indicative of the in-plane bending vibrations of the imidazole ring. Similarly, peaks at 1307, 1145, and 993 cm^{-1} are assigned to the in-plane bending signals of the imidazole ring, reinforcing the notion that these vibrational modes are integral to the structural integrity of ZIF-8 (Zhan et al., 2020). Additionally, C-H stretching vibrations are observed around 2930–2970 cm^{-1}, indicating

the presence of alkyl groups within the imidazole linkers. The absence of significant absorption bands beyond 3500 cm^{-1} suggests minimal surface hydroxylation or moisture adsorption, confirming that the bare ZIF-8 retains its structural integrity without notable modification by environmental exposure. Gr exhibited a broad absorption band between 3000–3500 cm^{-1}, which corresponds to O-H stretching, likely due to the presence of residual hydroxyl groups or adsorbed water, as noted by, The peak at 1700 cm^{-1} corresponds to the carbonyl group, consistent with previous findings by Zheng and co-workers, who reported similar carbonyl stretching vibrations in their analysis of rGO (A. L. T. Zheng, Boonyuen, Li, et al., 2021; A. L. T. Zheng, Boonyuen, Ohno, et al., 2021). Additionally, a prominent peak between 1560–1650 cm^{-1} is attributed to C=C stretching vibrations, confirming the presence of conjugated double bonds in the Gr structure. The weak peaks observed between 1000–1500 cm^{-1} suggest the existence of residual oxygen-containing groups, which could indicate incomplete reduction of GO, showing some retained oxygen functionalities in the graphitic material, a characteristic supported by (Fu et al., 2014). The FTIR spectrum of the ZIF-8/Gr shows a combination of features from both ZIF-8 and Gr, confirming successful integration of the two materials. The characteristic C–N stretching vibrations of ZIF-8 from the imidazole rings appeared to reduce in intensity. This is likely due to the interaction between the functional groups of Gr and the ZIF-8 framework, which can lead to a reduction in the intensity of specific FTIR peaks associated with ZIF-8, such as those related to the imidazole linkers (Jamil et al., 2021).

4.2 XRD Characterization

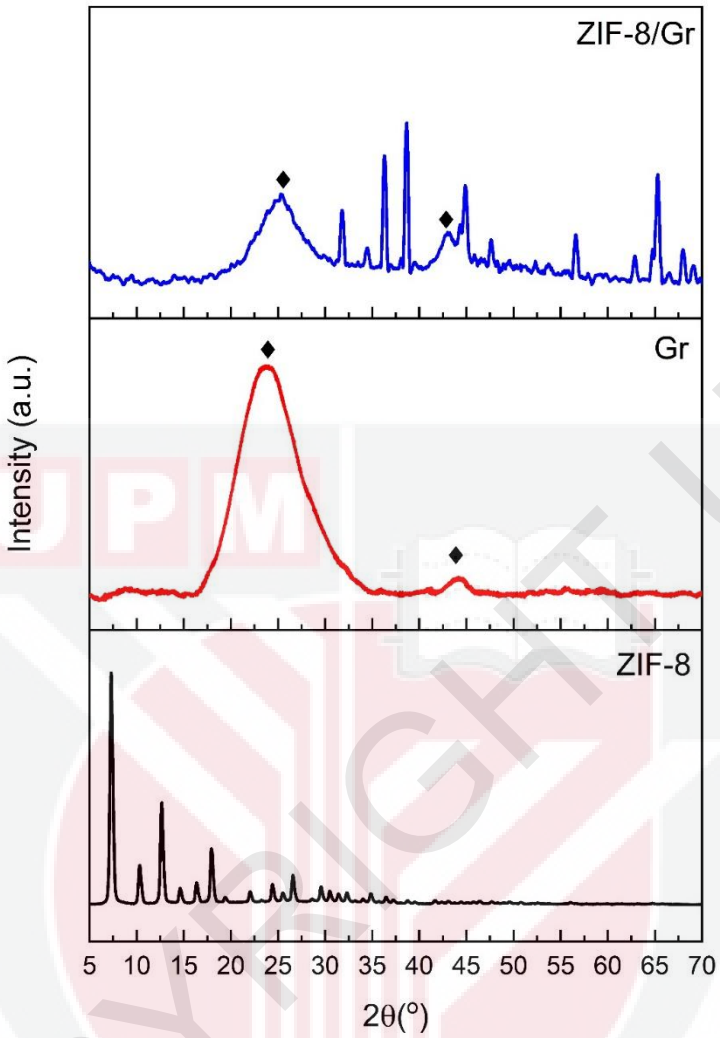

Fig. 4.2. XRD spectra of (a) bare ZIF-8 (b) Gr (c) ZIF-8/Gr.

XRD patterns of ZIF-8, Gr, and the ZIF-8/Gr composite are presented in Fig. 4.2 The XRD pattern of pure ZIF-8 displays sharp and intense peaks, particularly in the low-angle region (5°–20°), indicative of its high crystallinity. The prominent diffraction peaks at 7.3°, 10.4°, 12.7°, 14.7°, and 18.0° (2θ) are consistent with the cubic crystal structure of ZIF-8, as reported previously (S. Wang & Zhang, 2017). These peaks correspond to the (011), (002), (112), (022), and (013) planes, respectively, confirming the successful synthesis of ZIF-8. The crystalline size of ZIF-8 was estimated using the Debye-Scherrer equation, focusing on the most prominent peak at 2θ=7.3o. The calculation yielded a crystalline size of approximately 15.92 nm. The Gr exhibits a broad peak centered at approximately 26.3° (2θ), corresponding to the

(002) plane of graphitic carbon. The broad nature of this peak is indicative of disordered stacking of Gr layers and partial reduction of oxygen-containing groups. Additionally, a secondary peak at 44° is observed, attributed to the (101) plane, suggesting some retained graphitic domains (Chadha et al., 2021). This pattern confirms the presence of a partially reduced Gr structure with a mixture of amorphous and crystalline phases. The XRD pattern of the ZIF-8/Gr composite shows the characteristic peaks of both ZIF-8 and Gr. The peaks associated with ZIF-8 are still present but appear slightly diminished in intensity, suggesting a degree of interaction between the ZIF-8 framework and the Gr sheets. This could also indicate partial coverage or alteration of the ZIF-8 crystal structure due to the presence of Gr. Notably, the broad (002) peak of Gr at 26.3° overlaps with some ZIF-8 peaks, forming a combined signal indicative of the hybrid nature of the composite. This suggests the successful incorporation of ZIF-8 onto the Gr sheets without significant loss of its crystalline structure. The XRD analysis confirms the structural integrity of ZIF-8 and its successful integration with Gr to form the ZIF-8/Gr composite.

4.3 Morphological Characterization (SEM)

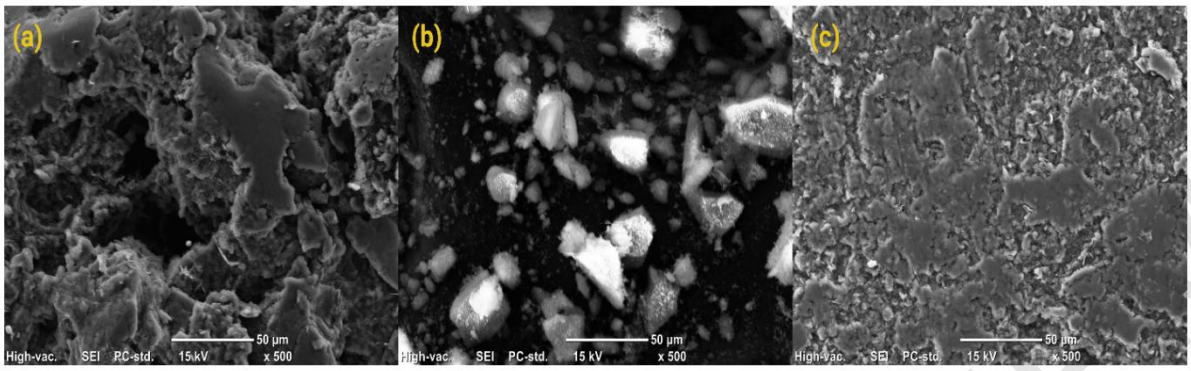

Fig. 4.3. SEM micrograph of (a) Gr (b) bare ZIF-8 (c) ZIF-8/Gr.

The morphological features of Gr, ZIF-8, and ZIF-8/Gr were examined using scanning electron microscopy (SEM), as shown in Fig. 4.3. respectively. Fig. 4.3 (a) displays the SEM image of reduced Gr, which reveals a characteristic wrinkled and sheet-like structure (Sethumadhavan et al., 2022; Viprya et al., 2023; Zheng et al., 2021). These morphological features are consistent with the inherent properties of Gr-based materials, providing a high surface area and structural flexibility. The wrinkled surface morphology of Gr facilitates the dispersion of ZIF-8 particles and offers abundant active sites for interaction, making it an ideal substrate for composite formation. Fig. 4.3 (b) shows the SEM image of ZIF-8, which displays irregularly shaped aggregates with a rough and porous surface morphology. Unlike the ideal polyhedral crystals commonly associated with ZIF-8, the observed structure indicates a deviation likely due to synthesis parameters or agglomeration effects (Xing et al., 2022). The rough surface and porosity suggest potential utility in adsorption and catalytic applications, as the increased surface area can provide enhanced interaction sites. The ZIF-8/Gr composite showed a homogeneous distribution of ZIF-8 particles on the Gr sheets as shown in Fig. 4.3 (c). The ZIF-8 aggregates are embedded within the Gr matrix, forming a well-integrated composite which enhanced the structural stability of the material This synergistic morphology is expected to improve the material's functional properties, such as their photocatalytic activity, (Y. Wang et al., 2021) and adsorption capacity. The ZIF-8/Gr composite micrograph shows a well-

integrated hybrid structure, where ZIF-8 particles are effectively dispersed and anchored onto the graphene sheets. This synergy combines ZIF-8's high surface area and porosity with graphene's conductive network, leading to enhanced electron transfer, increased stability, and reduced agglomeration within the composite. These structural attributes are expected to improve pollutant degradation efficiency by providing more accessible active sites and enhanced electron flow throughout the material. The combined properties of ZIF-8's framework stability and Gr's conductivity suggest that the ZIF-8/Gr composite could offer superior performance for environmental remediation, aligning well with this study's objectives to create an efficient, stable catalyst for the degradation of persistent organic pollutants.

4.4 Thermal Characterization (TGA)

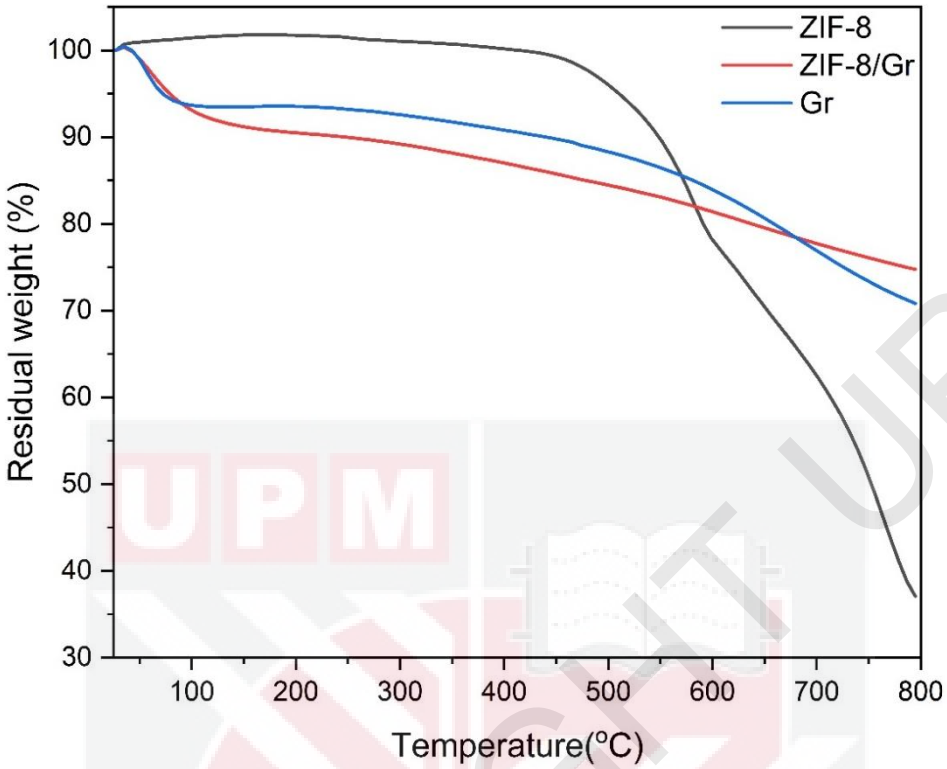

Fig. 4.4. TG thermogram of bare ZIF-8, Gr and ZIF-8/Gr.

The thermal stability of ZIF-8, Gr, and the ZIF-8/Gr composite was evaluated through TGA as shown in Fig. 4.4. The residual weight profiles for the three samples reveal distinct thermal behaviors, which can be attributed to their inherent material properties and interactions within the composite structure. The TGA curve of bare ZIF-8 exhibits two major stages of weight loss. The initial minor weight loss, observed below 150°C, corresponds to the desorption of physically adsorbed water and volatile organic compounds. Following this, the significant weight loss starting around 400°C is indicative of the thermal decomposition of the ZIF-8 framework (D. Huang et al., 2018). This decomposition corresponds to the collapse of the MOF structure, as the organic linkers decompose and volatilize, leaving behind residual zinc oxide. The TGA curve for Gr shows a gradual weight loss over the entire temperature range. The absence of significant weight loss at lower temperatures suggests minimal moisture or volatile

organic contamination in the sample. The gradual decline in weight, particularly from 400°C to 700°C, is attributed to the thermal degradation of graphitic carbon, possibly due to defects or edge sites in the Gr structure (Ikram et al., 2020). The final residual weight at 800°C is approximately 60%, highlighting Gr's superior thermal stability compared to ZIF-8. ZIF-8/Gr composite displays an intermediate thermal stability profile between those of bare ZIF-8 and Gr. The initial weight loss below 150°C, similar to Gr, is attributed to the desorption of physically adsorbed water. However, the subsequent weight loss, occurring between 400°C and 600°C, is less pronounced compared to bare ZIF-8. This reduced decomposition rate indicates enhanced thermal stability, likely due to the interaction between Gr and the ZIF-8 framework. The Gr acts as a stabilizing matrix, potentially mitigating the collapse of the MOF structure and delaying the thermal decomposition of the organic linkers. The final residual weight at 800°C is approximately 50%, which is higher than that of bare ZIF-8 but lower than Gr.

4.5 Optical Characterization

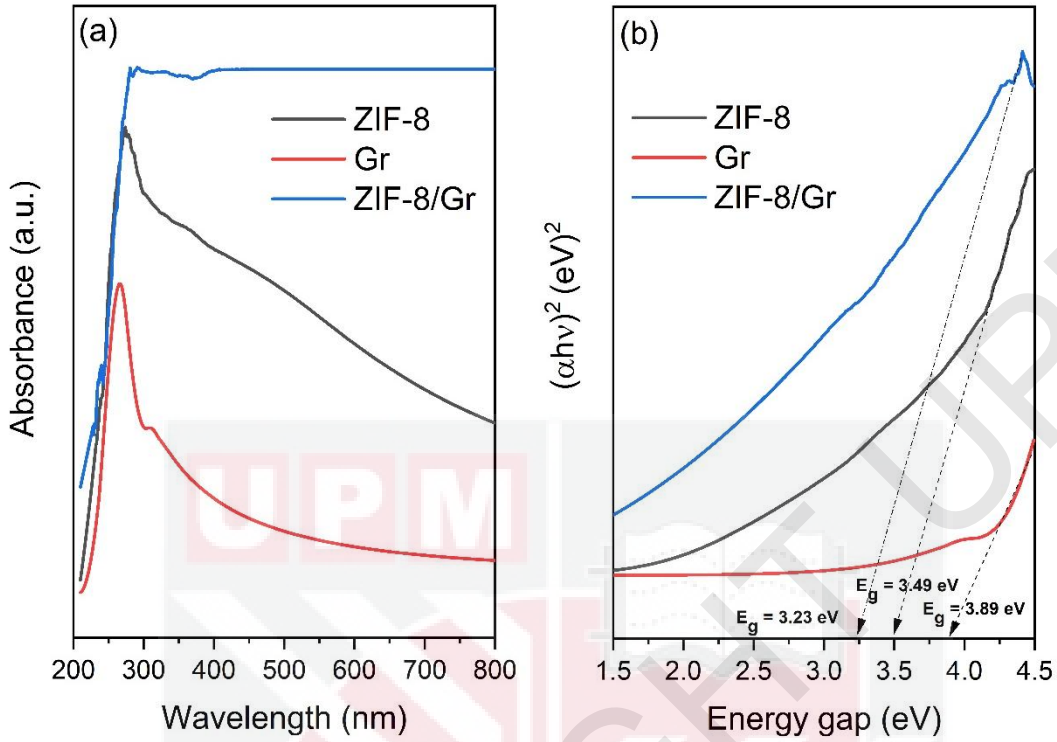

Fig. 4.5. (a) Band gap energy estimation (b) analysis by using Tauc plot.

The UV-Vis absorption spectra and the corresponding Tauc plots of ZIF-8, Gr and the ZIF-8/Gr composite are shown in Fig. 4.5. The absorption spectrum of ZIF-8 displays a distinct absorption band in the ultraviolet region below 300 nm, characteristic of its electronic transitions (Xiao et al., 2022). This is attributed to ligand-to-metal charge transfer (LMCT) within the ZIF-8 framework. The relatively sharp absorbance peak reflects the intrinsic properties of the ZIF-8 crystal structure. The reduced Gr exhibits a broader absorption profile, with a peak centered around 270 nm, corresponding to the π–π∗ transitions of the conjugated sp^2 bonded carbon framework (Emiru & Ayele, 2017; Zheng, Boonyuen, Li, et al., 2021). The broad nature of the spectrum across a wide range of wavelengths indicates its semiconducting properties with some optical absorption in the visible region. For the ZIF-8/Gr composite, the spectrum shows features from both ZIF-8 and Gr. The enhanced absorption across the UV and visible regions suggests strong interactions between ZIF-8 and the Gr, which enhance light absorption and broaden the composite's spectral response as shown in Fig. 4.5 (a). This synergistic effect can be attributed to the electronic coupling and interfacial charge transfer

between ZIF-8 and Gr. The E_g of the materials were calculated using the Tauc plot method, which involves plotting $(\alpha h\nu)^2$ versus photon energy (hv) and extrapolating the linear portion of the curve to the x-axis. The calculated E_g values for ZIF-8, Gr and ZIF-8/Gr is 3.89, 3.23 and 3.49 eV, respectively as shown in Fig. 4.5 (b). The intermediate band gap of ZIF-8/Gr reflects the synergistic interaction between ZIF-8 and Gr, likely resulting from charge transfer at the interface, which alters the electronic structure of the composite. The UV-Vis and Tauc plot analysis confirm the successful integration of ZIF-8 with Gr. The reduced band gap of the composite, compared to pure ZIF-8, implies improved light-harvesting properties and enhanced electronic interactions.

4.6 Photodegradation test

4.6.1 Comparison between bare and composite materials

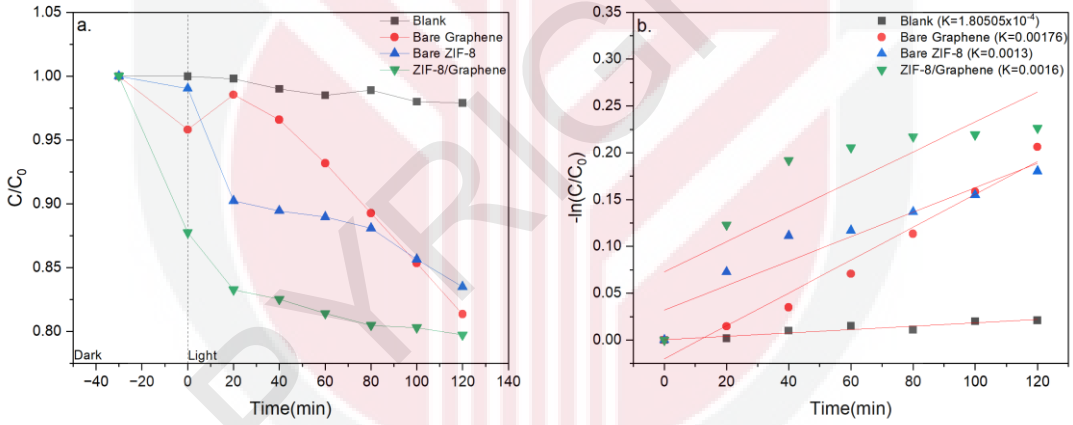

Fig. 4.6. (a) Photocatalytic degradation of LVX using various photocatalysts. **(b)** -ln (C/C_0) vs time.

The photocatalytic degradation performance of Gr, ZIF-8, and ZIF-8/Gr was evaluated over a 120-minute period under low-intensity UV light irradiation, preceded by a 30-minute dark phase to establish adsorption equilibrium. As shown in Fig. 4.6.(a), during the dark phase, adsorption of LVX onto the catalyst surfaces was observed, with ZIF-8/Gr exhibiting the highest adsorption capacity due to its enhanced surface area and abundant active sites provided by the synergistic interaction of ZIF-8 and Gr. This adsorption phase is crucial as it

ensures that any initial reduction in LVX concentration arises from adsorption alone, thereby providing a baseline for distinguishing between adsorption and photocatalytic mechanisms (X. Li et al., 2016; Samriti et al., 2022). ZIF-8/Gr demonstrated the highest degradation efficiency, achieving a C/C_0 value of 0.80, followed by Gr and ZIF-8 with values of 0.81 and 0.84, respectively. Gr, despite its remarkable electrical conductivity and high surface area, has limited intrinsic light absorption, which restricts its direct photocatalytic performance. Furthermore, its thin optical thickness and short-lived photogenerated carriers complicate photocurrent formation, further reducing its light absorption efficiency. Bare ZIF-8 recorded the lowest degradation rate and kinetic constant, a result of its poor stability in aqueous conditions (Jafari et al., 2024). The dissolution of ZIF-8 in water leads to the formation of zinc and imidazolate ions, which negatively impact its performance. Fig. 4.6(b) depicts the corresponding rate constants (k) calculated using pseudo-first-order (PFO) kinetics which follow the trend k (ZIF-8/Gr) > k (Gr) > k (ZIF-8). The superior performance of ZIF-8/Gr is attributed to the synergistic interaction between ZIF-8 and Gr, which improves charge separation, reduces electron-hole recombination, and facilitates the generation of ROS. While Gr's photocatalytic performance is inherently limited by its lack of efficient E_g, its high surface area and adsorption capacity enhance its overall activity. ZIF-8, by contrast, suffers from poor aqueous stability, which limits its standalone utility. Integrating Gr with ZIF-8 addresses these shortcomings by improving charge transport and providing additional active sites for pollutant adsorption and degradation.

4.6.2 Influence of amount of catalyst

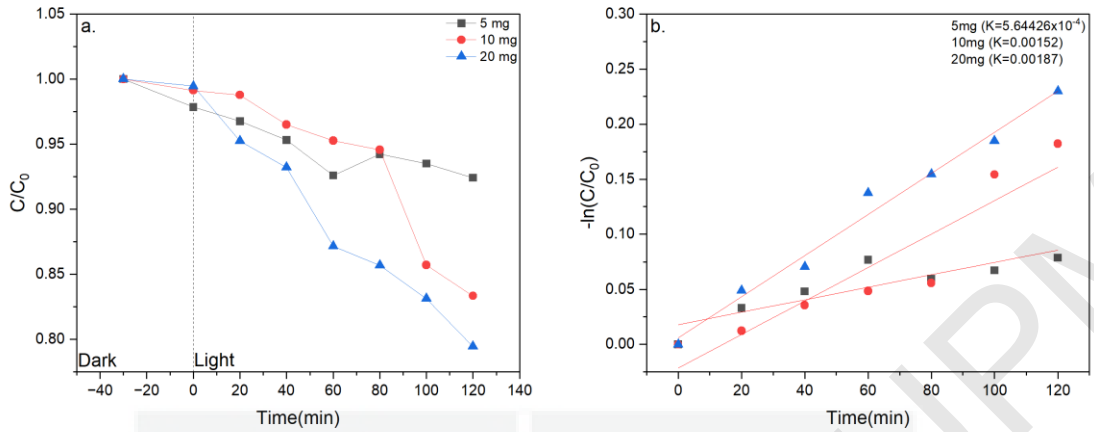

Fig. 4.7 (a) Influence of catalytic loading for LVX photodegradation. **(b)** -ln (C/C_0) vs time.

The amount of catalyst used in photocatalytic degradation plays a critical role in determining the efficiency and rate of the reaction. In this study, three different catalyst loadings of ZIF-8/Gr—5 mg, 10 mg, and 20 mg—were investigated for the photocatalytic degradation of LVX. The results presented in Fig. 4.7.(a) indicate a direct correlation between the amount of catalyst used and the efficiency of the photocatalytic degradation process. Increasing the catalyst loading from 5 mg to 20 mg led to a significant improvement in degradation efficiency. The findings aligned with existing literature, which suggests that insufficient catalyst quantities can result in suboptimal photocatalytic performance (Kaur et al., 2017). At 5 mg, the degradation efficiency was minimal, with a $-\ln(C/C_0)$ value of 0.08 and k of 5.64×10^{-4} min^{-1} after 120 minutes. Increasing the catalyst loading to 10 mg resulted in a $-\ln(C/C_0)$ value of 0.18 and a rate constant (k) value of 0.00152 min^{-1}, reflecting a notable enhancement in degradation efficiency. The highest loading of 20 mg achieved the maximum performance, with a $-\ln(C/C_0)$ value of 0.23 and a k value of 0.00187 min^{-1}. This enhanced performance is attributed to the increased availability of active sites, which facilitates greater generation of ROS and accelerates the photocatalytic degradation process (Iqbal et al., 2022). Higher catalyst concentrations generally promote faster reactions due to more efficient utilization of light and reactive species. However, beyond a certain threshold, further increases in catalyst

loading may lead to diminishing returns due to excessive turbidity in the reaction mixture, which scatters light and diminishes its effectiveness. High turbidity reduces light penetration, thereby decreasing the effective photon absorption and limiting the overall photocatalytic efficiency (D. Zhang et al., 2020). The degradation kinetics is depicted in Fig. 4.7(b). The results clearly indicate that increasing the catalyst loading from 5 mg to 20 mg resulted in a 3.3-fold increase in the rate constant, underscoring the direct relationship between catalyst loading and the rate of photocatalytic reactions.

4.6.3 Influence of initial concentration of LVX

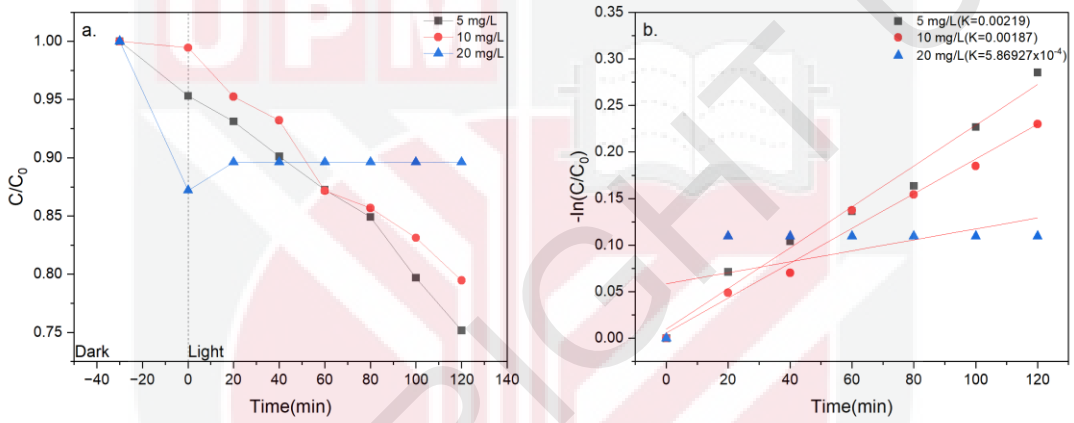

Fig. 4.8. (a) Influence of initial LVX concentration **(b)** -ln (C/C_0) vs time.

In this study, the influence of initial LVX concentrations on the photocatalytic degradation efficiency was evaluated using three concentrations: 5 mg/L, 10 mg/L, and 20 mg/L. The results presented in Fig.4.8. (a) demonstrate an inverse correlation between the initial pollutant concentration and the degradation efficiency. At a lower concentration of 5 mg/L, the degradation efficiency was the highest, with LVX concentration reducing to 3.686 mg/L after 120 minutes. For 10 mg/L, the degradation was moderately efficient, with the concentration dropping to 8.126 mg/L, while for 20 mg/L, the degradation was minimal, with the concentration stabilizing at 18.08 mg/L. This behaviour is attributed to the saturation of active sites on the catalyst surface at higher pollutant concentrations, which limits the degradation rate due to competitive adsorption and insufficient active sites. The degradation kinetics were

also analysed using the PFO model, as shown in Fig .4.8. (b). The rate constant (k) values decreased with increasing LVX concentration, reflecting reduced degradation efficiency at higher concentrations. Specifically, the k value was 0.00219 min^{-1} for 5 mg/L, 0.00187 min^{-1} for 10 mg/L, and 5.87 × 10^{-4} min^{-1} for 20 mg/L. These results indicate a significant 3.7-fold decrease in the rate constant when the initial LVX concentration increased from 5 mg/L to 20 mg/L. This trend highlights the critical role of pollutant concentration in determining the efficiency and kinetics of the photocatalytic process. The reduced efficiency at higher concentrations may also result from the absorption of incident light by LVX molecules, which reduces the light available for photocatalytic activation of the catalyst (Hadi et al., 2023).

4.6.4 Influence of pH

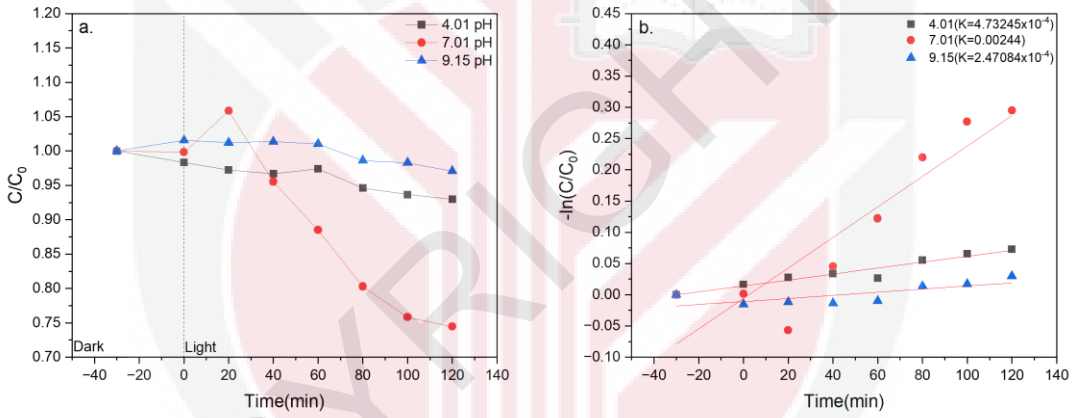

Fig. 4.9. (a) Influence of solution pH on LVX photodegradation. **(b)** -ln (C/C_0) vs time.

The effect of varying pH on the degradation rate of LVX and their kinetics is illustrated in Fig. 4.9. The degradation efficiency is highly influenced by the pH level of the solution. At a neutral pH of 7.01, the degradation rate is the highest, as the LVX concentration decreases significantly over time as shown in Fig. 4.9. (a). For example, after 120 minutes, the C/C_0 of LVX drops to 0.74, indicating effective degradation under neutral conditions. In contrast, at pH 4.01, the degradation is slower, with the C/C_0 decreasing only to 0.93. Similarly, at pH 9.15, the degradation rate is the slowest, with the C/C_0 stabilizing around 0.97, showing minimal change throughout the experimental period (Tayyebi et al., 2019). The slower degradation at

acidic and basic pH levels can be explained by the changes in the surface properties of the ZIF-8/Gr. Under acidic conditions, the catalyst's active sites may undergo protonation, reducing the interaction between the catalyst and the LVX molecules (Rincón & Pulgarin, 2004). In contrast, under basic conditions, the generation of hydroxyl ions may interfere with the formation of ROS, further impairing the photocatalytic activity (Rodríguez et al., 2011). Additionally, at basic pH, the increased concentration of hydroxyl ions may lead to competitive adsorption on the catalyst surface, further reducing the efficiency of the degradation process.

The degradation kinetics, as illustrated by the $-\ln(C/C_0)$ plot in Fig. 4.9. (b), exhibit trends that are consistent with the concentration-time profiles. At neutral pH, the degradation process adheres closely to pseudo-first-order kinetics, with a rate constant of 0.00283 min^{-1}, indicating a strong linear correlation between $-\ln(C/C_0)$ and time. This suggests efficient degradation due to favourable interactions between the catalyst and pollutant. In contrast, at acidic pH 4.01, the rate constant decreases to 5.62524×10^{-4} min^{-1}, indicating diminished degradation efficiency. The slowest degradation occurs under basic conditions pH 9.15, where the rate constant is further reduced to 3.11792×10^{-4} min^{-1}, highlighting a significant reduction in photocatalytic activity.

4.7 Radical trapping test

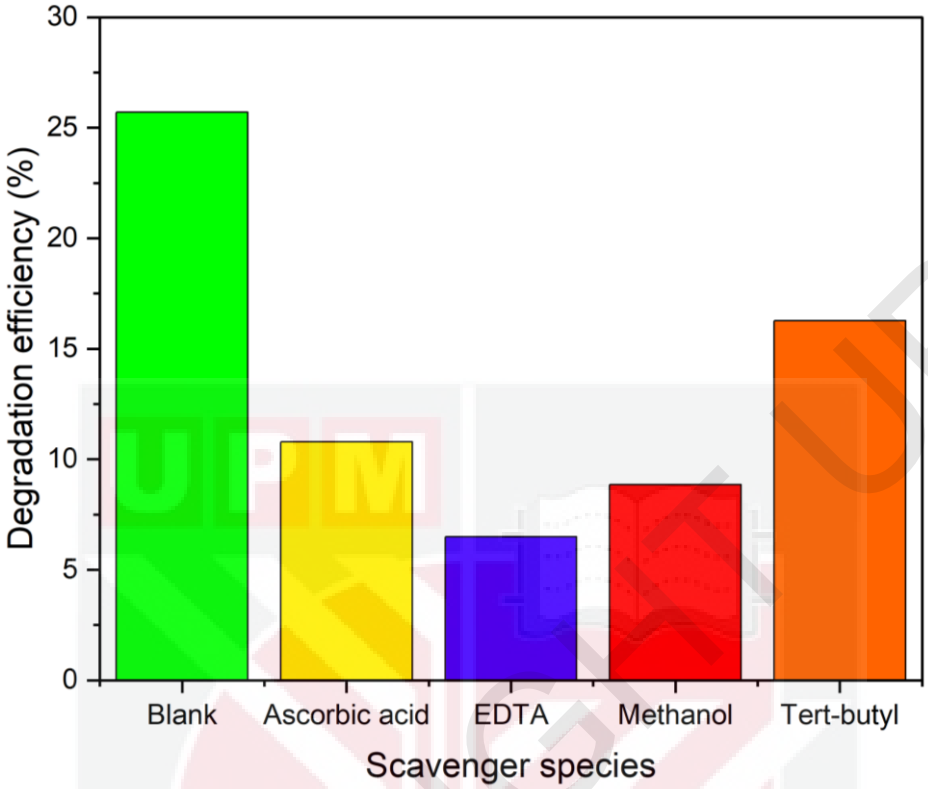

Fig. 4.10. Radical trapping test on photocatalytic degradation of LVX using ZIF-8/Gr.

The role of ROS in the photocatalytic degradation of LVX by ZIF-8/Gr was investigated using radical scavengers, as shown in Fig. 4.10. Various scavengers were introduced to assess the involvement of ($\bullet O_2^-$), ($\bullet OH$), and (h^+) in the degradation process, following similar approaches used in previous studies on radical trapping mechanisms (Luo et al., 2015). The baseline degradation efficiency without any scavenger was 26%, serving as a control for comparison. The addition of ascorbic acid, a known scavenger of $\bullet O_2^-$, led to a notable decrease in the degradation rate to around 10%, indicating that $\bullet O_2^-$ play a significant role in the degradation of LVX, consistent with findings from related work on the photocatalytic degradation of similar pollutants. EDTA, which effectively scavenges h^+, caused the most dramatic reduction in degradation, down to about 5%, suggesting that h^+ are a major contributor to the reaction mechanism. These findings aligned with prior studies emphasizing the importance of h^+ in catalytic degradation processes (Yu et al., 2022). On the other hand, the introduction of

methanol and tert-butyl alcohol, which are scavengers for •OH, resulted in more moderate reductions in degradation rates, approximately 10% and 15%, respectively. This suggests that •OH are involved in the degradation process but are not the primary reactive species compared to $•O_2^-$ and h^+. The results of the radical trapping experiments indicated that the degradation of LVX is primarily mediated by the following reactive species: $h^+ > •O_2^- > •OH$. These findings provide a basis for optimizing photocatalyst designs to enhance ROS production and improve overall degradation efficiency.

4.8 Regeneration test

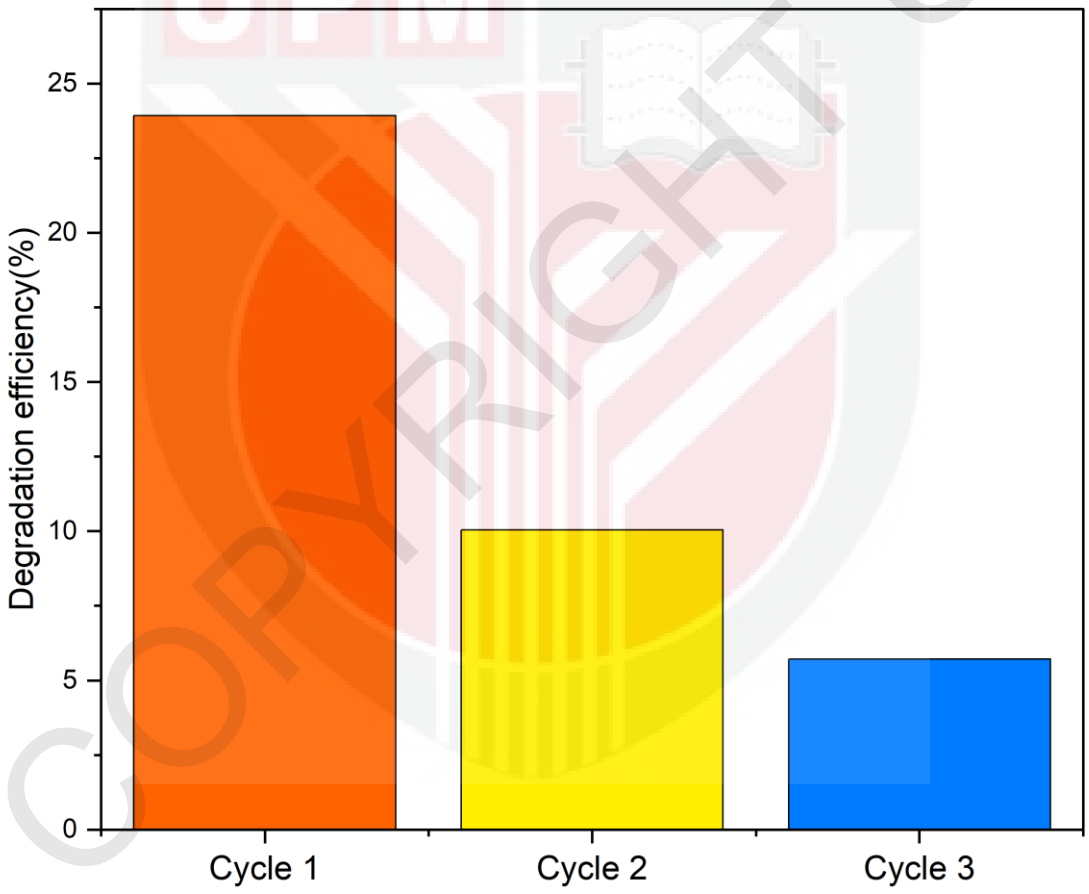

Fig. 4.11. Reusability and regeneration test of ZIF-8/Gr towards LVX degradation.

The reusability and stability of the ZIF-8/Gr composite catalyst were evaluated through three successive photocatalytic degradation cycles of LVX, as shown in Fig. 4.11. The initial LVX concentration was controlled at 5 mg/L, and the reaction conditions were kept constant to

assess the consistency of the photocatalytic degradation performance. After each trial, the catalyst was centrifuged at 4000 rpm to separate it from the water, washed with ethanol three times, and dried for 12 hours at 80°C to ensure reusability in subsequent trials. The initial degradation efficiency was 23.92% in the first cycle but decreased to 10.04% and 5.71% in the second and third cycles, respectively. This decline in performance can be attributed to potential catalyst deactivation caused by several factors, including the accumulation of residual by-products on the catalyst surface, incomplete regeneration during washing and drying, and structural degradation due to repeated use (Piera et al., 2002). Ethanol washing, while effective for initial cleaning, may have altered the surface structure of the ZIF-8/Gr composite, reducing its active sites and photocatalytic activity (Ataee Khorrami et al., 2024). Additionally, photo-corrosion or leaching of active components, commonly observed in some MOFs, could contribute to the observed reduction in catalytic performance over multiple cycles (Muelas-Ramos et al., 2021). Despite the decrease in degradation efficiency, the ZIF-8/Gr composite demonstrated adequate reusability for practical applications, as the catalyst retained a portion of its activity after three cycles. Further optimization of catalyst regeneration methods, such as alternative washing techniques or surface reactivation treatments, may improve its long-term stability. These findings highlight the importance of addressing catalyst durability to ensure sustained performance in large-scale photocatalytic applications.

4.9 Possible photodegradation mechanism of LVX

A potential photocatalytic degradation mechanism for the ZIF-8/Gr composite under low-power intensity UV light irradiation can be proposed as shown in Fig. 4.12.

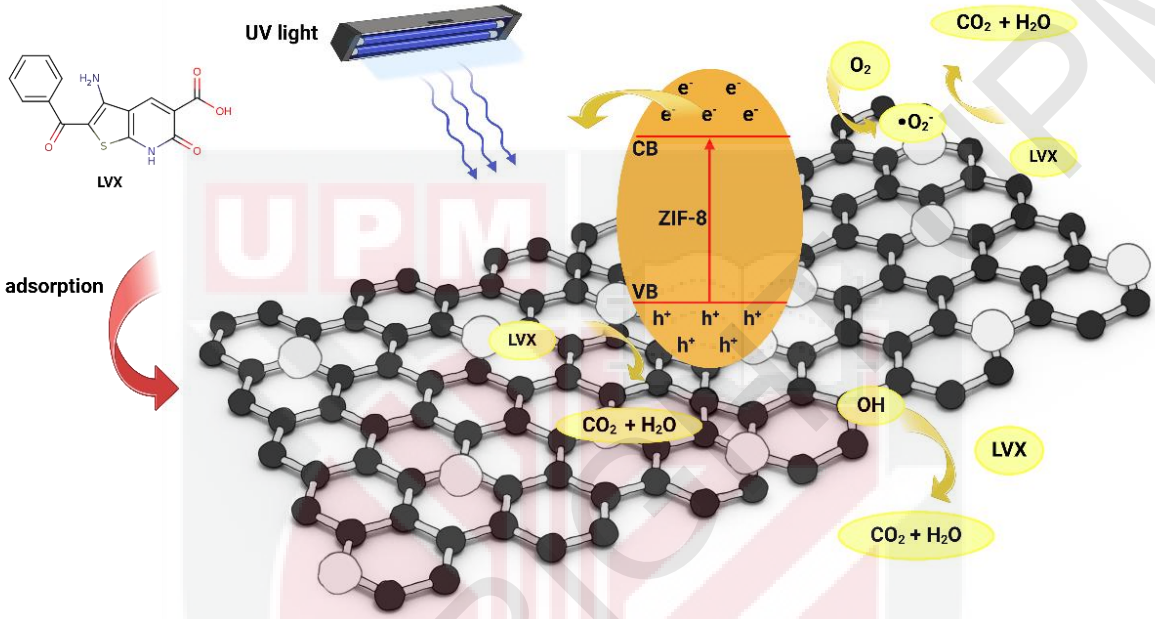

Fig. 4.12. Proposed LVX degradation mechanism.

A potential photocatalytic degradation mechanism for the ZIF-8/Gr composite under low-power intensity UV light irradiation can be proposed as shown in Fig.4.12. When exposed to UV light, electrons in the VB of ZIF-8 are excited to the CB, generating electron-hole pairs (e^-/h^+). The presence of Gr plays a crucial role in this process, acting as an electron percolation network (Tiong et al., 2015). This facilitates efficient electron transfer and enhances charge separation by suppressing the recombination of electron-hole pairs. The improved charge separation promotes the generation of ROS, which are essential for the photocatalytic degradation process. Specifically, the photogenerated holes (h^+) can interact with water molecules or hydroxide ions (OH^-) to produce •OH, which are highly reactive species capable of breaking down organic pollutants. According to radical trapping experiments, the primary ROS involved in the photocatalytic degradation were identified as •OH and h^+, indicating their dominant role

in the degradation mechanism. The degradation of LVX via this mechanism can be expressed through the following sequence of reactions:

1. Photoexcitation:

   ZIF-8/Gr + *hv* (UV light) → ZIF-8/Gr (e^- + h^+)

2. Charge separation enhancement by Gr:

   Gr reduces electron-hole recombination, improving the efficiency of charge carriers.

3. Reactive species formation:

   $h^+ + H_2O \rightarrow \bullet OH$

   $e^- + O_2 \rightarrow \bullet O_2^-$

4. Degradation of LVX:

   LVX + h^+/•OH /$\bullet O_2^-$→ Oxidized intermediates → $CO_2 + H_2O$

The photogenerated electrons in the CB may also contribute by reducing O_2 into $\bullet O_2^-$, further enhancing the formation of ROS that degrade LVX. Thus, the synergy between ZIF-8 and Gr plays a role in amplifying the efficiency of photocatalytic degradation under low intensity UV light. The possible degradation pathway of LVX during the photocatalytic reaction is also proposed based on literature and theoretical understanding (Prabavathi et al., 2021; Rameel et al., 2023). The degradation process begins with the excitation of ZIF-8/Gr under UV light, generating ROS that interact with the LVX, initiating oxidative breakdown at specific functional groups. The degradation starts with the decarboxylation of the methylmorpholine group in LVX resulting in a fragment with a molecular ion peak close to m/z = 336, indicating the loss of a carboxyl group. The degradation is followed by oxidation of the piperazine ring in which the N-methyl piperazine ring undergoes oxidation, forming a stable intermediate. Subsequently, de-alkylation reactions, defluorination and hydroxylation were predicted. The intermediates will undergo further oxidative cleavage, breaking down into small organic acids and eventually mineralizing into carbon dioxide and water. This hypothesized pathway highlights the stepwise

transformation of LVX into smaller intermediates, driven by the synergistic effects of ZIF-8/Gr. One previous study using visible-light-driven peroxymonosulfate activation over $CuInS_2$/g-C_3N_4 proposed four distinct LVX pathways (e.g., hydroxylation, fluorine removal, piperazine cleavage, and C-N bond cleavage) (X. Zhong et al., 2023). The proposed mechanism provides insights into how LVX undergoes oxidative degradation, emphasizing the role of ROS in breaking down complex structures into simpler, environmentally benign products. Although no LC-MS or GC-MS analyses were conducted in this study, a potential sequence of intermediate transformations is hypothesized to elucidate the degradation mechanism.

4.10 Antibacterial test

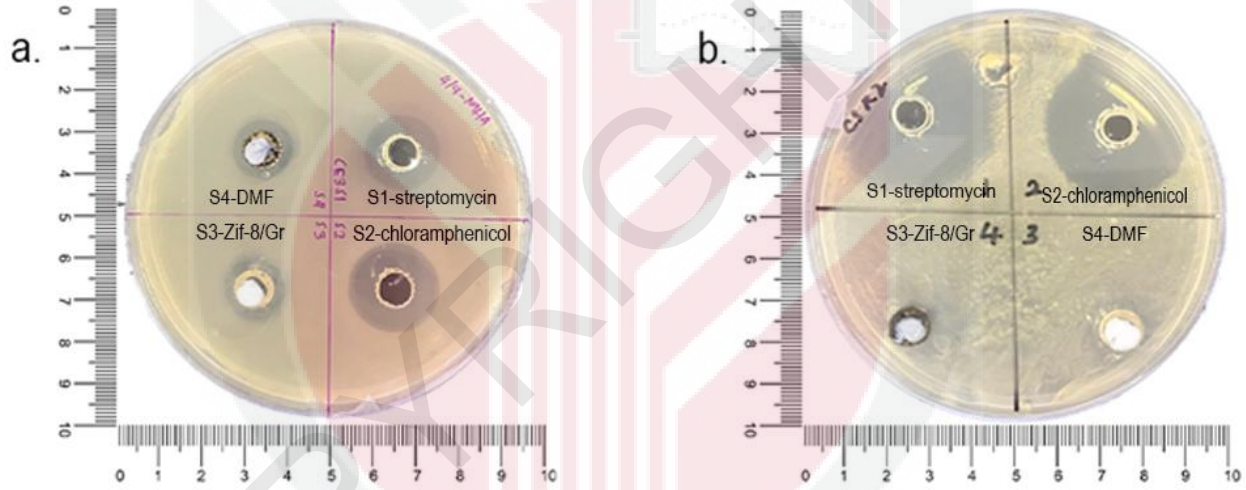

Fig. 4.13. Antibacterial activity against (a) *E. coli* and (b) *S. aureus* using ZIF-8/Gr.

The antibacterial activity of ZIF-8/Gr dissolved in DMF was evaluated against two bacterial strains: *E. coli* and *S. aureus*. The results, as depicted in Fig.4.13. and summarized in Table 1, indicate that ZIF-8/Gr exhibited a moderate antibacterial effect, particularly when compared to standard antibiotics such as chloramphenicol and streptomycin. The mechanical damage is a primary mechanism by which Gr exerts its bactericidal effects, as demonstrated by the ability of Gr nanospikes to physically rupture bacterial membranes and induce oxidative stress, which together enhance their antibacterial efficacy (A. L. T. Zheng, Farrag, et al., 2021). Previous study posited that the excellent antibacterial activity of GO based Co-MOF is linked

to synergistic effect of sharp edges of the GO sheets and the toxic effect of cobalt ions Co^{2+} which are released from their surfaces (Hatamie et al., 2019).

For *E. coli*, the ZIF-8/Gr composite exhibited notable antibacterial activity, with a ZOI measuring 1.4 ± 0.85 cm. This result indicates the material's potential to inhibit the growth of this Gram-negative bacterium. While the ZOI is smaller compared to conventional antibiotics like chloramphenicol and streptomycin, the results indicate that ZIF-8/Gr is still effective to some degree against *E. coli*. In contrast, for *S. aureus*, the ZIF-8/Gr results are considered negative in terms of antibacterial activity, with a ZOI of 0.9 ± 0.85 cm, which is quite low. This suggests that the material has little to no significant antibacterial effect against this Gram-positive bacterium (P. Li et al., 2019). The ZOI is much smaller compared to those of the control antibiotics, indicating that ZIF-8/Gr is not effective against *S. aureus*. The differential antibacterial activity of ZIF-8/Gr against *E. coli* and *S. aureus* can be attributed to several factors, including the structural differences between Gram-negative and Gram-positive bacteria, the specific properties of the ZIF-8/Gr, and the mechanisms of action involved. *E. coli* has an outer membrane that can act as a barrier to certain antibacterial agents, whereas *S. aureus*, lacks this outer membrane but has a thicker peptidoglycan layer (P. Li et al., 2019). It is important to note that DMF employed as a solvent control, exhibited minimal to no antibacterial activity, with ZOIs of 1.5 ± 0.80 cm for *E. coli* and 0.90 ± 0.85 cm for *S. aureus*. These findings reinforce the hypothesis that the observed antibacterial effects are attributable to the ZIF-8/Gr material itself, rather than the solvent (Chauhan et al., 2014). Overall, while ZIF-8/Gr shows potential as an antibacterial agent, further optimization may be required to enhance its effectiveness, particularly in comparison to established antibiotics.

Table 4.1: ZOI of ZIF-8/Gr towards *E. coli* and *S.aureus*

Sample	***Escherichia coli*** ***(E. coli)***	***Staphylococcus aureus*** ***(S. aureus)***
ZIF-8/Gr	1.4 ± 0.85	0.9 ± 0.85
Streptomycin	1.7 ± 0.80	3.8 ± 0.8
Chloramphenicol	2.2 ± 0.85	3.5 ± 0.7
Dimethylformamide	1.5 ± 0.80	0.90 ± 0.85

4.11 Antioxidant test

The DPPH assay was further used to evaluate the antioxidant activity of the ZIF-8/Gr composite, specifically its ability to scavenge free radicals, which are reactive species capable of causing cellular and tissue damage. As illustrated in Fig. 4.14. (a) and (b), no observable colour change was detected in the DPPH assay, indicating that ZIF-8/Gr does not effectively donate electrons to neutralize the DPPH radical. This result suggests that the material lacks significant antioxidant activity. In the context of photocatalytic applications, particularly in wastewater treatment, the absence of antioxidant properties in nanomaterials can be advantageous. A lack of electron-donating activity implies that the material will not neutralize ROS, which are essential for the degradation of organic pollutants. Therefore, the limited antioxidant activity of ZIF-8/Gr may enhance its photocatalytic efficiency by allowing the material to fully participate in ROS-driven reactions, which are critical for the breakdown of pollutants

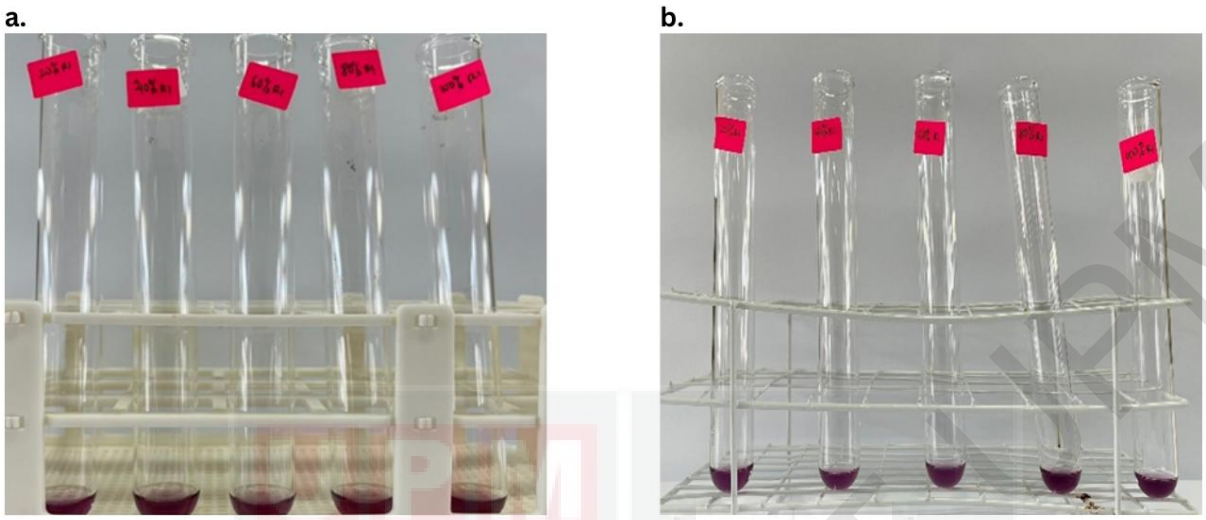

Fig. 4.14. Dose dependent decolorization of DPPH (20%, 40%, 60%, 80%, 100%) by ZIF-8/Gr dispersed in **(a)** DMF and **(b)** methanol.

Although Gr has previously been reported to exhibit antioxidant behaviour, this property is highly dependent on its surface chemistry. The antioxidant capabilities of Gr are closely tied to the presence of functional groups, such as hydroxyl or carboxyl groups, which facilitate interactions with free radicals (Demianenko et al., 2023). However, these functional groups were likely absent or reduced in the ZIF-8/Gr composite due to the hydrothermal treatment employed during synthesis, which may have significantly reduced oxygenated functional groups on the surface. These functional groups play a key role in the physical adsorption of superoxide anion radicals, thereby enhancing Gr's antioxidant capacity, ZIF-8, on the other hand, is primarily recognized for its catalytic and adsorption properties rather than its antioxidant potential. The Zn ions in ZIF-8, along with its imidazolate linkers, are not structurally equipped to engage in electron donation or free radical scavenging, which are typical mechanisms involved in antioxidant processes. Moreover, the structural stability of MOFs under oxidative conditions can be a limiting factor. For instance, Mn-based MOFs have demonstrated oxidative degradation under such conditions, which could compromise their

functionality (Khramenkova et al., 2018). Therefore, the absence of antioxidant properties in ZIF-8/Gr aligns with its design and purpose in photocatalysis rather than radical scavenging.

4.12 Cost analysis

The cost analysis for the synthesis of ZIF-8/Gr composite was conducted to evaluate its economic viability for potential large-scale applications. The synthesis of ZIF-8/Gr was evaluated for cost efficiency, yielding approximately 4.5 grams of the catalyst at a total production cost of RM 242.95, which corresponds to RM 53.99 per gram as shown in Table 2. This analysis considered the cost of all raw materials, including $Zn(NO_3)_2 \cdot 6H_2O$, 2-Methylimidazole and GO. The calculations were based on current market prices and the quantities of each material used in the optimized synthesis procedure. The total raw material cost is at RM 217.18. A key observation from this analysis is the significant contribution of Gr to the overall cost. While ZIF-8 synthesis itself is relatively inexpensive due to the readily available and affordable precursors, the incorporation of Gr substantially increases the final product cost. This cost increase is attributed to the more complex production processes and higher market value associated with Gr materials. This finding highlights a critical trade-off in the development of ZIF-8/Gr composites. While graphene imparts desirable properties such as improved stability, and increased surface area, its inclusion comes at a considerable economic premium. It is also important to note that economies of scale could potentially reduce the cost per gram in larger production runs. The hydrothermal method employed for synthesizing ZIF-8/Gr is energy-intensive (RM 6.48) but offers high yields and superior material properties, such as controlled crystallite size and phase purity. The operational costs associated with maintaining a reaction temperature of 180°C for 15 hours are a significant factor. The operational energy requirement for photocatalytic applications is notably low due to the catalyst's ability to function under low-intensity UV light. Using a low-power (13 W) UV lamp significantly reduces electricity costs, making this catalyst ideal for low-energy, environmentally friendly applications.

Table 4.2: Estimated costs involved in the synthesis of ZIF-8/Gr.

Item	Quantity (per batch)	Unit Cost (RM)	Total Cost (RM)	Notes
Raw Materials				
$Zn(NO_3)_2 \cdot 6H_2O$	1.78 g	0.196/g	0.34	ZIF-8 framework
2-Methylimidazole	5.26 g	1.87/g	9.84	Organic linker
Graphene Oxide (GO) suspension	9.00 g	23.00/g	207.00	
Total Raw Material Cost			**217.18**	
Synthesis Process				
Hydrothermal heating (180°C)	1.5 kWh X 18 hours = 27.0 kWh	RM 0.24 per kWh*	6.48	Energy cost for ZIF-8/Gr synthesis
Sonication	0.23 kWh X5 hours = 1.15 kWh	RM 0.24 per kWh*	0.27	
Deionized water	200 mL	RM0.01/mL	2.00	For dissolving reagents and washing catalyst
Methanol (for washing)	20 mL	RM 0.15/ mL	3.00	Used for ZIF-8 washing
Methanol (for washing)	20 mL	RM 0.11/ mL	2.20	Used for ZIF-8/Gr washing
Drying	1.5 kWh X 24 hours = 36.0 kWh	RM 0.24 per kWh*	8.64	Energy cost for oven operation

				for ZIF-8 and ZIF-8/Gr drying
Calcination	3.0 kWh X 4 hours = 12.0 kWh	RM 0.24 per kWh*	2.88	Energy cost for box furnace operation
Total Process Cost			**25.47**	
Equipment Depreciation				
Teflon-lined autoclave usage	-	-	0.20	Based on estimated equipment depreciation per batch
Centrifuge/filtration setup	-	-	0.10	Equipment for recovery and filtration
Total Equipment Cost			**0.30**	
Overall Synthesis Cost			**242.95**	Per batch (4.5 g photocatalyst yield)

Notes: *refer to Sarawak Energy tariff rate.

CHAPTER 5

CONCLUSION AND FUTURE WORKS

5.1 Conclusion

This study successfully demonstrated the photocatalytic degradation of LVX using a ZIF-8/Gr composite under low-intensity UV irradiation. The ZIF-8/Gr outperformed its individual components, achieving the highest degradation efficiency through improved charge separation, and superior production of ROS. The optimal degradation was achieved with 20 mg of catalyst applied to a 5 mg/L solution of LVX at neutral pH (7.01), resulting in a 25.70% degradation rate after 120 minutes of low-intensity UV exposure. Key ROS responsible for this enhanced degradation included •OH, $\bullet O_2^-$, and h^+, all of which contributed significantly to the oxidative breakdown of LVX. The degradation followed PFO kinetics, with lower pollutant concentrations enabling faster degradation rates due to improved interaction between the ZIF-8/Gr and LVX. Gr's role in enhancing electron transfer and minimizing electron-hole recombination was crucial to the composite's superior performance. The ZIF-8/Gr composite not only effectively degraded pollutants under low-intensity UV light but also exhibited antibacterial properties in the dark, as evidenced by the ZOI against *E. coli*. This dual functionality highlights the material's broader applicability, making it a promising candidate for wastewater treatment and environmental remediation. This study provides valuable insights into the development of advanced photocatalytic materials, advancing the potential for improved wastewater treatment technologies.

5.2 Future works

1. Optimization of synthesis conditions:

- Hydrothermal conditions: Investigate the optimal hydrothermal time and temperature to achieve the highest photocatalytic activity
- Precursor ratio: Explore different ratio of ZIF-8: Gr to control the distribution and dispersion of the photocatalysts

2. Catalyst Characterization:

- Structural Analysis: Conduct more detailed structural characterization using techniques like transmission electron microscopy (TEM), and Raman spectroscopy to elucidate the relationship between ZIF-8: Gr and the catalyst's structural properties.
- Electronic Properties: Investigate the electronic properties of ZIF-8/Gr, such as bandgap and charge carrier mobility, to gain a deeper understanding of its photocatalytic mechanism.

3. Performance Evaluation:

- Different Pollutants: Evaluate the performance of ZIF-8/Gr in degrading other antibiotic pollutants
- Real-World Applications: Test the catalyst in real-world wastewater treatment scenarios to assess its practical applicability and durability.

4. Mechanism Investigation:

- In-Situ Techniques: Employ in-situ techniques (e.g., electron paramagnetic resonance, transient absorption spectroscopy) to directly observe the formation and behaviour of reactive oxygen species during the degradation process.

References

Abukhadra, M. R., Mohamed, A. S., El-Sherbeeny, A. M., & Soliman, A. T. A. (2020). Enhanced Adsorption of Toxic and Biologically Active Levofloxacin Residuals from Wastewater Using Clay Nanotubes as a Novel Fixed Bed: Column Performance and Optimization. *ACS Omega*, *5*(40), 26195–26205. https://doi.org/doi/10.1021/acsomega.0c03785

Afroz, R., & Rahman, A. (2017). Health impact of river water pollution in Malaysia. *International Journal of Advanced and Applied Science*, *4*(5), 78–85. https://doi.org/10.21833/IJAAS.2017.05.014

Alansi, A. M., Qahtan, T. F., & Saleh, T. A. (2021). Solar-Driven Fixation of Bismuth Oxyhalides on Reduced Graphene Oxide for Efficient Sunlight-Responsive Immobilized Photocatalytic Systems. *Advanced Materials Interfaces*, *8*(3), 2001463. https://doi.org/10.1002/ADMI.202001463

Alvarino, T., Suarez, S., Lema, J., & Omil, F. (2018). Understanding the sorption and biotransformation of organic micropollutants in innovative biological wastewater treatment technologies. *Science of The Total Environment*, *615*, 297–306. https://doi.org/10.1016/J.SCITOTENV.2017.09.278

Arachchi, S. S., Palma, S. P., Sanders, C. I., Xu, H., Ghosh Biswas, R., Soong, R., Simpson, A. J., & Casabianca, L. B. (2023). Binding Between Antibiotics and Polystyrene Nanoparticles Examined by NMR. *ACS Environmental Au*, *3*(1), 47–55. https://doi.org/doi/10.1021/acsenvironau.2c00047

Ataee Khorrami, M., Sohrabnezhad, S., & Asadollahi, A. (2024). Enhanced visible-light-active MOF-based PbO photocatalyst for binary dye decolorization: A comprehensive study. *Journal of Molecular Liquids*, *402*, 124722. https://doi.org/10.1016/J.MOLLIQ.2024.124722

Atchudan, R., Edison, T. N. J. I., Perumal, S., Shanmugam, M., & Lee, Y. R. (2017). Direct solvothermal synthesis of zinc oxide nanoparticle decorated graphene oxide nanocomposite for efficient photodegradation of azo-dyes. *Journal of Photochemistry and Photobiology A: Chemistry*, *337*, 100–111. https://doi.org/10.1016/J.JPHOTOCHEM.2017.01.021

Autreto, P. A. S., De Sousa, J. M., & Galvao, D. S. (2014). Site-dependent hydrogenation on graphdiyne. *Carbon*, *77*, 829–834. https://doi.org/10.1016/J.CARBON.2014.05.088

Bhattacharyya, S., Sholl, D. S., & Nair, S. (2020). Quantitative Correlations for the Durability of Zeolitic Imidazolate Frameworks in Humid SO $_2$. *Industrial & Engineering Chemistry Research*, *59*(1), 245–252. https://doi.org/10.1021/acs.iecr.9b05787

Bobirică, L., Bobirică, C., Lupu, G. I., Orbeci, C., Manea, F., Ramona, T., & Ildyko, S. E. (2021). Influence of Operating Parameters on Photocatalytic Oxidation of 2,4-Dichlorofenol in Aqueous Solution by TiO2/Stainless Steel Photocatalytic Membrane. *Applied Sciences 2021, Vol. 11, Page 11664*, *11*(24), 11664. https://doi.org/10.3390/APP112411664

Bouider, B., Haffad, S., Bouakaz, B. S., Berd, M., Ouhnia, S., & Habi, A. (2023). MOF-5/Graphene Oxide Composite Photocatalyst for Enhanced Photocatalytic Activity of Methylene Blue Degradation Under Solar Light. *Journal of Inorganic and Organometallic Polymers and Materials*, *33*(12), 4001–4011. https://doi.org/10.1007/s10904-023-02668-y

Chadha, N., Sharma, R., & Saini, P. (2021). A new insight into the structural modulation of graphene oxide upon chemical reduction probed by Raman spectroscopy and X-ray diffraction. *Carbon Letters*, *31*(6), 1125–1131. https://doi.org/10.1007/s42823-021-00234-5

Chauhan, H. P. S., Carpenter, J., & Joshi, S. (2014). Mixed bis(morpholine-4-dithiocarbamato-S,S′)antimony(III) complexes: synthesis, characterization and biological studies. *Applied Organometallic Chemistry*, *28*(8), 605–613. https://doi.org/10.1002/AOC.3169

Chemello, G., Knigge, X., Ciornii, D., Reed, B. P., Pollard, A. J., Clifford, C. A., Howe, T., Vyas, N., Hodoroaba, V. D., & Radnik, J. (2023). Influence of the Morphology on the Functionalization of Graphene Nanoplatelets Analyzed by Comparative Photoelectron Spectroscopy with Soft and Hard X-Rays. *Advanced Materials Interfaces*, *10*(20), 2300116. https://doi.org/10.1002/ADMI.202300116

Chen, H., Xu, H., & Dong, W. (2018). Preparation and Photocatalytic Properties of Ag2CO3 / Graphene Composite Photocatalyst. *Journal of Analytical Chromatography and Spectroscopy*, *1*(1). https://doi.org/10.24294/jacs.v1i1.346

Cincinelli, A., Martellini, T., Coppini, E., Fibbi, D., & Katsoyiannis, A. (2015). Nanotechnologies for Removal of Pharmaceuticals and Personal Care Products from Water and Wastewater. A Review. *Journal of Nanoscience and Nanotechnology*, *15*(5), 3333–3347. https://doi.org/10.1166/JNN.2015.10036

Demianenko, E., Sencha-Hlevatska, K., Sementsov, Y., & Kartel, M. (2023). Quantum-chemical investigation of the superoxide radical scavenging by graphene oxide surface. *Low Temperature Physics*, *49*(9), 1088–1092. https://doi.org/10.1063/10.0020603

Doğan, V., Isık, T., Kılıç, V., & Horzum, N. (2022). A field-deployable water quality monitoring with machine learning-based smartphone colorimetry. *Analytical Methods*, *14*(35), 3458–3466. https://doi.org/10.1039/D2AY00785A

Edokpayi, J. N., Enitan, A. M., Mutileni, N., & Odiyo, J. O. (2018). Evaluation of water quality and human risk assessment due to heavy metals in groundwater around Muledane area of Vhembe District, Limpopo Province, South Africa. *Chemistry Central Journal*, *12*(1), 1–16. https://doi.org/10.1186/S13065-017-0369-Y/TABLES/7

Fu, H., Qu, X., Chen, W., & Zhu, D. (2014). Transformation and destabilization of graphene oxide in reducing aqueous solutions containing sulfide. *Environmental Toxicology and Chemistry*, *33*(12), 2647–2653. https://doi.org/10.1002/ETC.2730

Fukidome, H., Nagashio, K., Nagamura, N., Tashima, K., Funakubo, K., Horiba, K., Suemitsu, M., Toriumi, A., & Oshima, M. (2014). Pinpoint operando analysis of the electronic states of a graphene transistor using photoelectron nanospectroscopy. *Applied Physics Express*, *7*(6), 065101. https://doi.org/10.7567/APEX.7.065101/XML

Grandclément, C., Seyssiecq, I., Piram, A., Wong-Wah-Chung, P., Vanot, G., Tiliacos, N., Roche, N., & Doumenq, P. (2017). From the conventional biological wastewater treatment to hybrid processes, the evaluation of organic micropollutant removal: A review. *Water Research*, *111*, 297–317. https://doi.org/10.1016/J.WATRES.2017.01.005

Guo, R., Xing, Y., Liu, M., Bai, T., Pu, C., & Zhang, H. (2021). Facile synthesis of BIVO4@ZIF-8 composite with heterojunction structure for photocatalytic wastewater treatment. *Materials*, *14*(23), 7424. https://doi.org/10.3390/MA14237424/S1

Guo, X., He, S., Meng, Z., Wang, Y., & Peng, Y. (2022). Ag@ZIF-8/g-C3N4 Z-scheme photocatalyst for the enhanced removal of multiple classes of antibiotics by integrated adsorption and photocatalytic degradation under visible light irradiation. *RSC Advances*, *12*(28), 17919–17931. https://doi.org/10.1039/D2RA02194C

Hadi, A., Niaei, A., Seifi, A., & Rasoulzadeh, Y. (2023). The impact of operational factors on degradation of formaldehyde as a human carcinogen using Ag3 PO4 /TiO2 photocatalyst. *Health Promotion Perspectives*, *13*(1), 47–53. https://doi.org/10.34172/hpp.2023.06

Han, C. S., Kang, J. H., Park, E. hye, Lee, H. J., Jeong, S. J., Kim, D. W., & Park, C. W. (2023). Corrugated surface microparticles with chitosan and levofloxacin for improved aerodynamic performance. *Asian Journal of Pharmaceutical Sciences*, *18*(3), 100815. https://doi.org/10.1016/J.AJPS.2023.100815

Han, X., Zhang, T., Cui, Y., Wang, Z., Dong, R., Wu, Y., Du, C., Chen, R., Yu, C., Feng, J., Sun, J., & Dong, S. (2023). A Bifunctional BiOBr/ZIF-8/ZnO Photocatalyst with Rich Oxygen Vacancy for Enhanced Wastewater Treatment and H2O2 Generation. *Molecules*, *28*(6), 2422. https://doi.org/10.3390/MOLECULES28062422/S1

Hatamie, S., Ahadian, M. M., Soufi Zomorod, M., Torabi, S., Babaie, A., Hosseinzadeh, S., Soleimani, M., Hatami, N., & Wei, Z. H. (2019). Antibacterial properties of nanoporous graphene oxide/cobalt metal organic framework. *Materials Science and Engineering: C*, *104*, 109862. https://doi.org/10.1016/J.MSEC.2019.109862

He, J., Ye, J., Zhang, Y., Kong, L., Zhou, X., Ma, Y., & Yang, Y. (2020). Synergistic RGO/Black TiO2/2D-ZIF-8 Ternary Heterogeneous Composite with Highly Efficient Photocatalytic Activity. *ChemistrySelect*, *5*(12), 3746–3755. https://doi.org/10.1002/SLCT.201904939

Heltina, D., Randa, D. G., A Naufal, M. B., & Partama, A. (2022). Performance evaluation of graphene (CTAB)/TiO2/Fe3O4 composite on phenol degradation. *Rasayan J. Chem*, *15*(3), 2022. https://doi.org/10.31788/RJC.2022.1536857

Heu, R., Ateia Ibrahim, M., & Yoshimura, C. (2018). *Adsorption Capacity of UiO-66 Enhanced by Graphene Oxide for Carbamazepine Removal in Water*. https://www.researchgate.net/publication/350467504

Heu, R., Ateia, M., Yoshimura, C., Awfa, D., & Punyapalakul, P. (2020). Photocatalytic degradation of organic micropollutants in water by zr-mof/go composites. *Journal of Composites Science*, *4*(2). https://doi.org/10.3390/jcs4020054

Huang, A., Yan, M., Lin, J., Xu, L., Gong, H., & Gong, H. (2021). A Review of Processes for Removing Antibiotics from Breeding Wastewater. *International Journal of Environmental Research and Public Health 2021, Vol. 18, Page 4909*, *18*(9), 4909. https://doi.org/10.3390/IJERPH18094909

Huang, D., Xin, Q., Ni, Y., Shuai, Y., Wang, S., Li, Y., Ye, H., Lin, L., Ding, X., & Zhang, Y. (2018). Synergistic effects of zeolite imidazole framework@graphene oxide composites in humidified mixed matrix membranes on CO2 separation. *RSC Advances*, *8*(11), 6099–6109. https://doi.org/10.1039/C7RA09794H

Huang, L., & Liu, B. (2016). Synthesis of a novel and stable reduced graphene oxide/MOF hybrid nanocomposite and photocatalytic performance for the degradation of dyes. *RSC Advances*, *6*(22), 17873–17879. https://doi.org/10.1039/C5RA25689E

Ikram, R., Jan, B. M., & Ahmad, W. (2020). An overview of industrial scalable production of graphene oxide and analytical approaches for synthesis and characterization. *Journal of*

Materials Research and Technology, *9*(5), 11587–11610. https://doi.org/10.1016/J.JMRT.2020.08.050

Iqbal, R. M. A., Akhtar, T., Sitara, E., Nasir, H., Fazal, A., Rafique, U., Ullah, S., & Mehmood, A. (2022). Development of Ag0.04ZrO2/rGO heterojunction, as an efficient visible light photocatalyst for degradation of methyl orange. *Scientific Reports 2022 12:1*, *12*(1), 1–12. https://doi.org/10.1038/s41598-022-16673-7

Jafari, S., Pourmortazavi, S. M., Ehsani, A., & Mirsadeghi, S. (2024). CuO-ZIF-8 modified electrode surface as a new electrochemical sensing platform for detection of free chlorine in aqueous solution. *Scientific Reports*, *14*(1), 18961. https://doi.org/10.1038/s41598-024-69869-4

Jafri, N. N. M., Jaafar, J., Aziz, F., Salleh, W. N. W., Yusof, N., Othman, M. H. D., Rahman, M. A., Ismail, A. F., Rahman, R. A., & Khongnakorn, W. (2022). Development of Free-Standing Titanium Dioxide Hollow Nanofibers Photocatalyst with Enhanced Recyclability. *Membranes 2022, Vol. 12, Page 342*, *12*(3), 342. https://doi.org/10.3390/MEMBRANES12030342

Jamil, N., Othman, N. H., Mohd Zaini, M. H., Alias, N. H., Shahruddin, M. Z., Lau, W. J., Ismail, A. F., & Md Nordin, N. A. H. (2021). Green one-pot synthesis and characterisation of hybrid reduced graphene oxide/zeolitic imidazole framework-8 (rGO/ZIF-8). *Journal of the Iranian Chemical Society*, *18*(2), 363–373. https://doi.org/10.1007/s13738-020-02032-8

Jeon, S. G., Ko, J. W., & Ko, W. B. (2021). Ultrasound assisted synthesis of gadolinium oxide-zeolitic imidazolate framework-8 nanocomposites and their optimization for photocatalytic degradation of methyl orange using response surface methodology. *Catalysts*, *11*(9), 1022. https://doi.org/10.3390/CATAL11091022/S1

Jiang, X., Zhang, H., Wang, X., Zhang, X., & Ding, K. (2022). Comprehensive Analysis of the Association between Human Diseases and Water Pollutants. *International Journal of Environmental Research and Public Health 2022, Vol. 19, Page 16475*, *19*(24), 16475. https://doi.org/10.3390/IJERPH192416475

Kaur, A., Salunke, D. B., Umar, A., Mehta, S. K., Sinha, A. S. K., & Kansal, S. K. (2017). Visible light driven photocatalytic degradation of fluoroquinolone levofloxacin drug using Ag2O/TiO2 quantum dots: a mechanistic study and degradation pathway. *New Journal of Chemistry*, *41*(20), 12079–12090. https://doi.org/10.1039/C7NJ02053H

Khan, Z. H., Kermany, A. R., Öchsner, A., & Iacopi, F. (2017). Mechanical and electromechanical properties of graphene and their potential application in MEMS. *Journal of Physics D: Applied Physics*, *50*(5), 053003. https://doi.org/10.1088/1361-6463/50/5/053003

Khramenkova, E. V., Polynski, M. V., Vinogradov, A. V., & Pidko, E. A. (2018). Degradation paths of manganese-based MOF materials in a model oxidative environment: a computational study. *Physical Chemistry Chemical Physics*, *20*(32), 20785–20795. https://doi.org/10.1039/C8CP00397A

Kodali, V. K., Scrimgeour, J., Kim, S., Hankinson, J. H., Carroll, K. M., De Heer, W. A., Berger, C., & Curtis, J. E. (2011). Nonperturbative chemical modification of graphene for protein micropatterning. *Langmuir*, *27*(3), 863–865. https://doi.org/doi/10.1021/la1033178

Kumar, A., Rana, A., Sharma, G., Naushad, M., Al-Muhtaseb, A. H., Guo, C., Iglesias-Juez, A., & Stadler, F. J. (2018). High-Performance Photocatalytic Hydrogen Production and Degradation of Levofloxacin by Wide Spectrum-Responsive Ag/Fe 3 O 4 Bridged SrTiO 3 /g-C 3 N 4 Plasmonic Nanojunctions: Joint Effect of Ag and Fe 3 O 4. *ACS Applied Materials and Interfaces*, *10*(47), 40474–40490. https://doi.org/doi/10.1021/acsami.8b12753

Lan, J., Wang, Y., Huang, B., Xiao, Z., & Wu, P. (2021). Application of polyoxometalates in photocatalytic degradation of organic pollutants. *Nanoscale Advances*, *3*(16), 4646–4658. https://doi.org/10.1039/D1NA00408E

Li, P., Li, J., Feng, X., Li, J., Hao, Y., Zhang, J., Wang, H., Yin, A., Zhou, J., Ma, X., & Wang, B. (2019). Metal-organic frameworks with photocatalytic bactericidal activity for integrated air cleaning. *Nature Communications 2019 10:1*, *10*(1), 1–10. https://doi.org/10.1038/s41467-019-10218-9

Li, X., Yu, J., Wageh, S., Al-Ghamdi, A. A., & Xie, J. (2016). Graphene in Photocatalysis: A Review. *Small*, *12*(48), 6640–6696. https://doi.org/10.1002/SMLL.201600382

Liu, A., Zhou, W., Shen, K., Liu, J., & Zhang, X. (2015). One-pot hydrothermal synthesis of hematite-reduced graphene oxide composites for efficient removal of malachite green from aqueous solution. *RSC Advances*, *5*(22), 17336–17342. https://doi.org/10.1039/C4RA15589K

Liu, L., Zhou, L., Liu, D., Yuan, W., Chen, S., Li, H., Bian, Z., Wang, J., & Wang, Z. L. (2021). Improved Degradation Efficiency of Levofloxacin by a Self-Powered Electrochemical System with Pulsed Direct-Current. *ACS Nano*, *15*(3), 5478–5485. https://doi.org/10.1021/acsnano.1c00233

Liu, N., Huang, W., Zhang, X., Tang, L., Wang, L., Wang, Y., & Wu, M. (2018). Ultrathin graphene oxide encapsulated in uniform MIL-88A(Fe) for enhanced visible light-driven photodegradation of RhB. *Applied Catalysis B: Environmental*, *221*, 119–128. https://doi.org/10.1016/J.APCATB.2017.09.020

Liu, P., Zhang, H., Feng, Y., Yang, F., & Zhang, J. (2014). Removal of trace antibiotics from wastewater: A systematic study of nanofiltration combined with ozone-based advanced oxidation processes. *Chemical Engineering Journal*, *240*, 211–220. https://doi.org/10.1016/J.CEJ.2013.11.057

Liu, Y., Cai, D., Li, X., Wu, Q., Ding, P., Shen, L., Yang, J., Hu, G., & Wu, J. (2022). Occurrence, fate, and risk assessment of antibiotics in typical pharmaceutical manufactories and receiving surface waters from different regions. *MedRxiv*, 2022.06.22.22276743. https://doi.org/10.1101/2022.06.22.22276743

Liu, Y., Dong, X., & Chen, P. (2012). Biological and chemical sensors based on graphene materials. *Chemical Society Reviews*, *41*(6), 2283–2307. https://doi.org/10.1039/C1CS15270J

Liu, Z., Li, Y., Li, C., Thummavichai, K., Feng, C., Li, Z., Liu, S., Zhang, S., Wang, N., & Zhu, Y. (2022). MOF-derived biochar composites for enhanced high performance photocatalytic degradation of tetracycline hydrochloride. *RSC Advances*, *12*(49), 31900–31910. https://doi.org/10.1039/D2RA05819G

Luo, J., Zhou, X., Zhang, J., & Du, Z. (2015). Fabrication and characterization of Ag2CO3/SnS2 composites with enhanced visible-light photocatalytic activity for the

degradation of organic pollutants. *RSC Advances*, *5*(105), 86705–86712. https://doi.org/10.1039/C5RA18262J

Ma, Z., Guan, B., Guo, J., Chen, Y., Chen, J., Dang, H., Zhu, C., Chen, L., Shu, K., Shi, K., Li, Y., Guo, Z., Yi, C., Hu, J., Hu, X., & Huang, Z. (2023). Synthesis of ZIF-8@TiO $_2$ Nanoribbon Catalysts by Ultrasonication for Enhanced Photocatalytic CO $_2$ Reduction Activity. *Industrial & Engineering Chemistry Research*, *62*(43), 17658–17670. https://doi.org/10.1021/acs.iecr.3c02726

Mu, C., Jian, S., & Zhang, M. (2024). Metal-Organic Frameworks (MOFs) and Metal-Organic Cages (MOCs) for Photocatalytic Hydrogen Production. *Chemistry – A European Journal*, *30*(43), e202401264. https://doi.org/10.1002/CHEM.202401264

Muelas-Ramos, V., Belver, C., Rodriguez, J. J., & Bedia, J. (2021). Synthesis of noble metal-decorated NH2-MIL-125 titanium MOF for the photocatalytic degradation of acetaminophen under solar irradiation. *Separation and Purification Technology*, *272*, 118896. https://doi.org/10.1016/J.SEPPUR.2021.118896

Nguyen, H. L. (2021). Metal–Organic Frameworks for Photocatalytic Water Splitting. *Solar RRL*, *5*(7), 2100198. https://doi.org/10.1002/SOLR.202100198

Novoselov, K. S., Fal'Ko, V. I., Colombo, L., Gellert, P. R., Schwab, M. G., & Kim, K. (2012). A roadmap for graphene. *Nature 2012 490:7419*, *490*(7419), 192–200. https://doi.org/10.1038/nature11458

Oberoi, A. S., Jia, Y., Zhang, H., Khanal, S. K., & Lu, H. (2019). Insights into the Fate and Removal of Antibiotics in Engineered Biological Treatment Systems: A Critical Review. *Environmental Science and Technology*, *53*(13), 7234–7264. https://doi.org/doi/10.1021/acs.est.9b01131

Owa, F. W. (2014). Water Pollution: Sources, Effects, Control and Management. *International Letters of Natural Sciences*, *8*, 1–6. https://doi.org/10.56431/P-GK4D9J

Paliwal, S., & Shorgar, N. (2023). Removal of Azure a Dye From Aqueous Solutions By Using Strontium Chromate-Zinc Oxide Nanocomposite. *Poll Res*, *42*(2), 248–254. https://doi.org/10.53550/PR.2023.v42i02.011

Pang, F., He, M., & Ge, J. (2015). Controlled Synthesis of Fe3O4/ZIF-8 Nanoparticles for Magnetically Separable Nanocatalysts. *Chemistry – A European Journal*, *21*(18), 6879–6887. https://doi.org/10.1002/CHEM.201405921

Piera, E., Ayllón, J., Doménech, X., & Peral, J. (2002). TiO2 deactivation during gas-phase photocatalytic oxidation of ethanol. *Catalysis Today*, *76*(2–4), 259–270. https://doi.org/10.1016/S0920-5861(02)00224-9

Prabavathi, S. L., Saravanakumar, K., Park, C. M., & Muthuraj, V. (2021). Photocatalytic degradation of levofloxacin by a novel Sm6WO12/g-C3N4 heterojunction: Performance, mechanism and degradation pathways. *Separation and Purification Technology*, *257*, 117985. https://doi.org/10.1016/j.seppur.2020.117985

Rameel, M. I., Wali, M., Al-Humaidi, J. Y., Liaqat, F., & Khan, M. A. (2023). Enhanced photocatalytic degradation of levofloxacin over heterostructured C3N4/Nb2O5 system under visible light. *Heliyon*, *9*(10), e20479. https://doi.org/10.1016/j.heliyon.2023.e20479

Rincón, A. G., & Pulgarin, C. (2004). Effect of pH, inorganic ions, organic matter and H2O2 on E. coli K12 photocatalytic inactivation by TiO2: Implications in solar water disinfection.

Applied Catalysis B: Environmental, *51*(4), 283–302. https://doi.org/10.1016/j.apcatb.2004.03.007

Rodríguez, E. M., Fernández, G., Álvarez, P. M., Hernández, R., & Beltrán, F. J. (2011). Photocatalytic degradation of organics in water in the presence of iron oxides: Effects of pH and light source. *Applied Catalysis B: Environmental*, *102*(3–4), 572–583. https://doi.org/10.1016/j.apcatb.2010.12.041

Saha, S., Jana, M., Samanta, P., Chandra Murmu, N., Kim, N. H., Kuila, T., & Lee, J. H. (2014). Hydrothermal synthesis of Fe3O4/RGO composites and investigation of electrochemical performances for energy storage applications. *RSC Advances*, *4*(84), 44777–44785. https://doi.org/10.1039/C4RA07388F

Saliba, D., Ammar, M., Rammal, M., Al-Ghoul, M., & Hmadeh, M. (2018). Crystal Growth of ZIF-8, ZIF-67, and Their Mixed-Metal Derivatives. *Journal of the American Chemical Society*, *140*(5), 1812–1823. https://doi.org/doi/10.1021/jacs.7b11589

Samriti, Manisha, Chen, Z., Sun, S., & Prakash, J. (2022). Design and engineering of graphene nanostructures as independent solar-driven photocatalysts for emerging applications in the field of energy and environment. *Molecular Systems Design & Engineering*, *7*(3), 213–238. https://doi.org/10.1039/D1ME00179E

Sanchez, V. C., Jachak, A., Hurt, R. H., & Kane, A. B. (2012). Biological interactions of graphene-family nanomaterials: An interdisciplinary review. *Chemical Research in Toxicology*, *25*(1), 15–34. https://doi.org/doi/10.1021/tx200339h

Santika, N., & W, D. L. (2021). Water Pollution Analysis in Yogyakarta Special Region In 2019. *Journal of International Conference Proceedings*, *4*(3), 153–160. https://doi.org/10.32535/JICP.V4I3.1306

Senapati, D., Swain, J., & Priyadarshini, A. (2024). *Photocatalytic Dye Degradation by ZIF-8@BiVO4 Composite*. https://doi.org/10.21203/RS.3.RS-4599818/V1

Tayyebi, A., Soltani, T., & Lee, B. K. (2019). Effect of pH on photocatalytic and photoelectrochemical (PEC) properties of monoclinic bismuth vanadate. *Journal of Colloid and Interface Science*, *534*, 37–46. https://doi.org/10.1016/j.jcis.2018.08.095

Tiong, P., Lintang, H. O., Endud, S., & Yuliati, L. (2015). Improved interfacial charge transfer and visible light activity of reduced graphene oxide–graphitic carbon nitride photocatalysts. *RSC Advances*, *5*(114), 94029–94039. https://doi.org/10.1039/C5RA17967J

Tiwari, A., Kapoor, R., Jain, J., & Sankhla, J. (2022). *Water Purifications Methods in Ayurveda and Contemporary Methods*. *10*. https://doi.org/10.22214/ijraset.2022.47137

Varma, K. S., Shukla, A. D., Tayade, R. J., Joshi, P. A., Das, A. K., Modi, K. B., & Gandhi, V. G. (2022). Photocatalytic performance and interaction mechanism of reverse micelle synthesized Cu-TiO2 nanomaterials towards levofloxacin under visible LED light. *Photochemical & Photobiological Sciences*, *21*(1), 77–89. https://doi.org/10.1007/s43630-021-00141-8

Wang, J., & Wang, S. (2018). Microbial degradation of sulfamethoxazole in the environment. *Applied Microbiology and Biotechnology*, *102*(8), 3573–3582. https://doi.org/https://doi.org/10.1007/s00253-018-8845-4

Wang, P., Li, R., Cheng, X., Wang, Y., Wang, Q., Wu, Z., An, B., Zhang, T., Yang, Y., & Xie, E. (2023). High Response of ZIF-8-Derived ZnO Nanorods to Low-Concentration Ethylene Glycol. *ACS Applied Nano Materials*, *6*(23), 22069–22079. https://doi.org/10.1021/acsanm.3c04268

Wang, Q., Wang, G., Xie, S., Zhao, X., & Zhang, Y. (2019). Comparison of high-performance liquid chromatography and ultraviolet-visible spectrophotometry to determine the best method to assess Levofloxacin released from mesoporous silica microspheres/nano-hydroxyapatite composite scaffolds. *Experimental and Therapeutic Medicine*. https://doi.org/10.3892/etm.2019.7238

Wang, S., & Zhang, S. (2017). Study on the Structure Activity Relationship of ZIF-8 Synthesis and Thermal Stability. *Journal of Inorganic and Organometallic Polymers and Materials*, *27*(5), 1317–1322. https://doi.org/10.1007/s10904-017-0585-x

Wang, Y., Zheng, Y., Zhao, G., Liu, S., Hu, J., Long, X., Xiao, Z., Zhang, H., & Jiao, F. (2021). Co-precipitation synthesis of reusable ZnAl-CLDH/ZIF-8 heterojunction for enhanced photodegradation of organic dye. *Journal of Materials Science: Materials in Electronics*, *32*(24), 28051–28064. https://doi.org/10.1007/s10854-021-07118-4

Wu, J., Wu, D., Peng, W., Ji, Y., & Tong, H. (2022). Research progress of polyoxometalates photocatalyst for degradation of organic wastewater. *Applied Chemical Engineering*, *5*(1), 92–106. https://doi.org/10.24294/ACE.V5I1.1635

Wu, Y., Luo, H., & Wang, H. (2014). Synthesis of iron(iii)-based metal-organic framework/graphene oxide composites with increased photocatalytic performance for dye degradation. *RSC Advances*, *4*(76), 40435–40438. https://doi.org/10.1039/c4ra07566h

Xia, Y., Shang, S., Zeng, X., Zhou, J., & Li, Y. (2019). A Novel Bi2MoO6/ZIF-8 Composite for Enhanced Visible Light Photocatalytic Activity. *Nanomaterials*, *9*(4), 545. https://doi.org/10.3390/nano9040545

Xian, T., Yang, H., Di, L., Ma, J., Zhang, H., & Dai, J. (2014). Photocatalytic reduction synthesis of SrTiO3-graphene nanocomposites and their enhanced photocatalytic activity. *Nanoscale Research Letters*, *9*(1), 327. https://doi.org/10.1186/1556-276X-9-327

Xian, T., Yang, H., Wang, Y. F., Di, L. J., Jiang, J. L., Li, R. S., & Feng, W. J. (2014). Visible-Light Photocatalysis of LSMO-Graphene Nanocomposites toward Degradation of Methyl Red. *MATERIALS TRANSACTIONS*, *55*(2), 245–248. https://doi.org/10.2320/matertrans.M2013317

Xu, X., Zou, Q., Yuan, Y., Ji, F., Fan, Z., & Zhou, B. (2014). Preparation of BiVO4-Graphene Nanocomposites and Their Photocatalytic Activity. *Journal of Nanomaterials*, *2014*(1), 401697. https://doi.org/10.1155/2014/401697

Yang, C., You, X., Cheng, J., Zheng, H., & Chen, Y. (2017). A novel visible-light-driven In-based MOF/graphene oxide composite photocatalyst with enhanced photocatalytic activity toward the degradation of amoxicillin. *Applied Catalysis B: Environmental*, *200*, 673–680. https://doi.org/10.1016/J.APCATB.2016.07.057

Yang, X., Cao, G., Liu, H., Wang, C., Li, X., & Song, Z. (2021). Construction of mesoporous C3N4/rGO composite with enhanced visible light photocatalytic activity. *Optik*, *241*, 167159. https://doi.org/10.1016/J.IJLEO.2021.167159

Yu, Z., Lv, Y., Huang, F., Zhang, F., Shi, Q., An, K., Fan, T., Li, G., & Wang, J. (2022). Photoatalytic Degradation of Organic Pollutants in Water Under Visible Light by NH2-MIL-125(Ti-Zr)@BiOClxI1-x Composite Photocatalyst. *ChemistrySelect*, *7*(28), e202201958. https://doi.org/10.1002/SLCT.202201958

Zeng, L., Guo, X., He, C., & Duan, C. (2016). Metal-Organic Frameworks: Versatile Materials for Heterogeneous Photocatalysis. *ACS Catalysis*, *6*(11), 7935–7947. https://doi.org/doi/10.1021/acscatal.6b02228

Zeng, X., Huang, L., Wang, C., Wang, J., Li, J., & Luo, X. (2016). Sonocrystallization of ZIF-8 on Electrostatic Spinning TiO $_2$ Nanofibers Surface with Enhanced Photocatalysis Property through Synergistic Effect. *ACS Applied Materials & Interfaces*, *8*(31), 20274–20282. https://doi.org/10.1021/acsami.6b05746

Zhan, Y., Wang, Y., Wang, M., Ding, X., & Wang, X. (2020). Improving the Curing and Mechanical Properties of Short Carbon Fibers/Epoxy Composites by Grafting Nano ZIF-8 on Fibers. *Advanced Materials Interfaces*, *7*(2), 1901490. https://doi.org/10.1002/ADMI.201901490

Zhang, D., Lv, S., & Luo, Z. (2020). A study on the photocatalytic degradation performance of a [KNbO3]0.9-[BaNi0.5Nb0.5O3−δ]0.1 perovskite. *RSC Advances*, *10*(3), 1275–1280. https://doi.org/10.1039/C9RA07310H

Zhang, T., Wang, X., & Zhang, X. (2014). Recent Progress in TiO2-Mediated Solar Photocatalysis for Industrial Wastewater Treatment. *International Journal of Photoenergy*, *2014*(1), 607954. https://doi.org/10.1155/2014/607954

Zheng, A. L. T., Boonyuen, S., Li, G. Y., Ngee, L. H., & Andou, Y. (2021). Design of reduced graphene hydrogel with alkylamine surface functionalization through immersion/agitation method and its adsorption mechanism. *Journal of Molecular Structure*, *1245*, 131008. https://doi.org/10.1016/j.molstruc.2021.131008

Zheng, A. L. T., Boonyuen, S., Ohno, T., & Andou, Y. (2021). Hydrothermally Reduced Graphene Hydrogel Intercalated with Divalent Ions for Dye Adsorption Studies. *Processes*, *9*(1), 169. https://doi.org/10.3390/pr9010169

Zheng, A. L. T., Farrag, H. N., Sabidi, S., Kato, T., Maeda, T., & Andou, Y. (2021). Accessing the anti-microbial activity of cyclic peptide immobilized on reduced graphene oxide. *Materials Letters*, *304*, 130621. https://doi.org/10.1016/j.matlet.2021.130621

Zheng, S., Wang, Y., Chen, C., Zhou, X., Liu, Y., Yang, J., Geng, Q., Chen, G., Ding, Y., & Yang, F. (2022). Current Progress in Natural Degradation and Enhanced Removal Techniques of Antibiotics in the Environment: A Review. *International Journal of Environmental Research and Public Health 2022, Vol. 19, Page 10919*, *19*(17), 10919. https://doi.org/10.3390/IJERPH191710919

Zhong, W. L., Ma, B. Bin, Han, J., Chen, L. Y., Jing-Jing, S., Zhang, G. S., & Lei, C. X. (2024). Design of TiO2/ZIF-8 heterojunction with enhanced visible-light photocatalytic activity under mild conditions. *Journal of the Chinese Chemical Society*, *71*(2), 128–139. https://doi.org/10.1002/JCCS.202300414

Zhong, X., Ji, M., Wu, W., Lu, C., Liu, W., & Jiang, F. (2023). Enhanced Degradation of Levofloxacin through Visible-Light-Driven Peroxymonosulfate Activation over CuInS2/g-C3N4 Heterojunctions. *Nanomaterials*, *14*(1), 74. https://doi.org/10.3390/nano14010074

Zhou, F., & Zhu, Y. (2012). Significant photocatalytic enhancement in methylene blue degradation of Bi2WO6 photocatalysts via graphene hybridization. *Journal of Advanced Ceramics*, *1*(1), 72–78. https://doi.org/10.1007/s40145-012-0008-y

Zou, C., Geng, Q. J., Zhu, J. T., Jing, C., Zhong, W., & Hou, Z. S. (2021). Effects of KBr and KI on Photocatalytic Degradation of Dye W-7G with Nano-TiO2as Catalyst. *International Journal of Photoenergy*, *2021*. https://doi.org/10.1155/2021/6610093

Zouzelka, R., Remzova, M., Plsek, J., Brabec, L., & Rathousky, J. (2019). Immobilized rGO/TiO2 Photocatalyst for Decontamination of Water. *Catalysts 2019, Vol. 9, Page 708*, *9*(9), 708. https://doi.org/10.3390/CATAL9090708

Supplementary Materials

Fig. S1. Calibration (mg L^{-1})

BIOGRAPHY OF THE STUDENT

Author (s) : Calvin Manasseh A/L Manivel

Year of Publication	: January 2025
Title of the Work	: Assessing the Photocatalytic Performance of ZIF-8/Graphene Towards Levofloxacin
Bachelor	: Science in Industrial Chemistry with Honours
Department	: Science and Technology
Faculty	: Humanities, Management, and Science
Institution	: Universiti Putra Malaysia Bintulu Campus

Calvin Manasseh A/L Manivel is a driven and detail-oriented individual with a strong academic background in environmental and industrial chemistry. He holds a Bachelor's Degree in Science in Industrial Chemistry with Honours from Universiti Putra Malaysia Bintulu Campus. Prior to his undergraduate studies, Calvin completed a Diploma in Agricultural Engineering at Universiti Putra Malaysia Kampus Bintulu, where he built a solid scientific foundation and cultivated a passion for environmental technology and sustainability.

During his undergraduate program, Calvin conducted research on the photocatalytic degradation of levofloxacin using ZIF-8/Graphene composite materials. His thesis, titled *"Assessing the Photocatalytic Performance of ZIF-8/Graphene Towards Levofloxacin,"* explores the synthesis and application of advanced photocatalysts for tackling pharmaceutical pollutants in water. His work demonstrates a keen understanding of material chemistry, photocatalytic processes, and analytical techniques such as XRD, FTIR, UV-Vis, and FESEM.

Calvin’s hands-on experience with the fabrication and characterization of ZIF-8/Graphene composites, along with his ability to assess their photocatalytic efficiency under various conditions, has prepared him for a career in environmental research and industrial applications. He is passionate about creating innovative and sustainable solutions for water treatment and pollution control. Calvin’s academic dedication, research capabilities, and problem-solving mindset highlight his potential to contribute significantly to the field of industrial chemistry.